Evolution of the Northeastern Margin of the Kazakhstan Paleocontinent: Results of a Petro-Geochemical Study of Sedimentary and Volcanogenic-Sedimentary Rocks of the Zharma-Saur Isl...

Article *in* Geotectonics · October 2024

DOI: 10.1134/S0016852124700274

CITATIONS
0

READS
31

7 authors, including:

Valeria Penkina
Sobolev Institute of Geology and Mineralogy, Russian Academy of Sciences
2 PUBLICATIONS **0** CITATIONS
SEE PROFILE

Pavel Kotler
Sobolev Institute of Geology and Mineralogy, Russian Academy of Sciences
51 PUBLICATIONS **364** CITATIONS
SEE PROFILE

Inna Safonova
Southwest Jiaotong University
154 PUBLICATIONS **6,106** CITATIONS
SEE PROFILE

Sergey V. Khromykh
Sobolev Institute of Geology and Mineralogy, Russian Academy of Sciences
79 PUBLICATIONS **958** CITATIONS
SEE PROFILE

ISSN 0016-8521, Geotectonics, 2024, Vol. 58, No. 3, pp. 321–343. © Pleiades Publishing, Ltd., 2024.

Evolution of the Northeastern Margin of the Kazakhstan Paleocontinent: Results of a Petro-Geochemical Study of Sedimentary and Volcanogenic-Sedimentary Rocks of the Zharma-Saur Island Arc Zone

V. A. Penkina[a], P. D. Kotler[a, c, *], I. Yu. Safonova[a, b], S. V. Khromykh[a], A. A. Perfilova[a, b], A. V. Kulikova[a, c], and I. A. Galimullin[c]

[a] *Sobolev Institute of Geology and Mineralogy, Siberian Branch, Russian Academy of Sciences, Novosibirsk, 630090 Russia*
[b] *Novosibirsk State University, Novosibirsk, 630090 Russia*
[c] *Kazan Federal University, Kazan, 420111 Russia*
**e-mail: pkotler@yandex.ru*

Received January 31, 2024; revised March 19, 2024; repeatedly revised June 5, 2024; accepted June 26, 2024

Abstract—The petrography, petrochemistry, geochemistry, and Nd isotopy of sedimentary and volcanogenic-sedimentary rocks, as well as U–Pb dating of detrital zircons from sandstones and tuff sandstones of four stratigraphic units of the Zharma-Saur island arc zone, were carried out. The data obtained, geological structure, and analysis of discriminant diagrams indicate that the formation of sandstones of the Givetian–Frasnian unit was the result of erosion and destruction of Early Paleozoic igneous complexes of the Chingiz-Tarbagatai zone of the Kazakhstan Paleocontinent. Tuff sandstones of the Koyanda Formation of the Tournaisian Stage and the Tersairyk Formation of the Visean Stage, distributed within the Vorontsov-Saur subzone, are a product of rock destruction and volcanic activity of the Zharma-Saur volcanic arc. The Early Paleozoic formations of the Chingiz-Tarbagatai zone and the Early Carboniferous volcanogenic complexes of the Zharma-Saur volcanic arc were simultaneously the provinces for the sedimentary rocks of the Kokon' Formation of the Visean Stage, which occupies most of the Zharma-Sarsazan subzone. Our data show that the Zharma-Saur arc was emplaced at the northeastern margin of the Kazakhstan Paleocontinent at the end of the Late Devonian–in the Early Carboniferous.

Keywords: island arc, volcanism, provenance area, Zharma-Saur zone, Late Paleozoic, Eastern Kazakhstan
DOI: 10.1134/S0016852124700274

INTRODUCTION

The Zharma-Saur island arc zone (hereafter, Zharma-Saur zone) of Eastern Kazakhstan is located in the western part of the Central Asian orogenic belt (CAOB). This zone is the conjunction area of the Early Paleozoic complexes of the Boshchekul-Chingiz folded area, which forms the northeastern part of the Kazakhstan Paleocontinent and the Late Paleozoic complexes of the Ob'-Zaisan (Irtysh-Zaisan) folded area (Fig. 1). The eastern part of the Zharma-Saur zone is composed of Late Paleozoic volcanogenic-sedimentary complexes of island arc origin; the western part represents a Carboniferous sedimentary trough that formed on the Early Paleozoic basement [7].

At present, several different geodynamic models for the development of the Zharma-Saur zone and the northeastern margin of the Kazakhstan Paleocontinent during the Devonian-Carboniferous period have been proposed [7, 11, 34, 35, 41, 58, 60, 64, 65]. The models differ both in the direction of the subduction of the oceanic plate—to the southwest towards the Boshchekul-Chingiz folded area complexes or to the northeast towards the Siberian continent; in the relative position of the Zharma-Saur arc relative to the Kazakhstan Paleocontinent – the volcanic arc functioned at a distance or on the edge of the Kazakhstan Paleocontinent. The models are considered in more detail in the geological essay.

The present study aims to conduct a comprehensive analysis of data obtained from sedimentary and volcanogenic-sedimentary sequences of the Zharma-Saur zone of Eastern Kazakhstan, including determining the composition of provenances, to refine the interval of island arc magmatism, and to determine the age of rocks in the provinces northeastern margin of the Kazakhstan Paleocontinent in the Devonian–Carboniferous period.

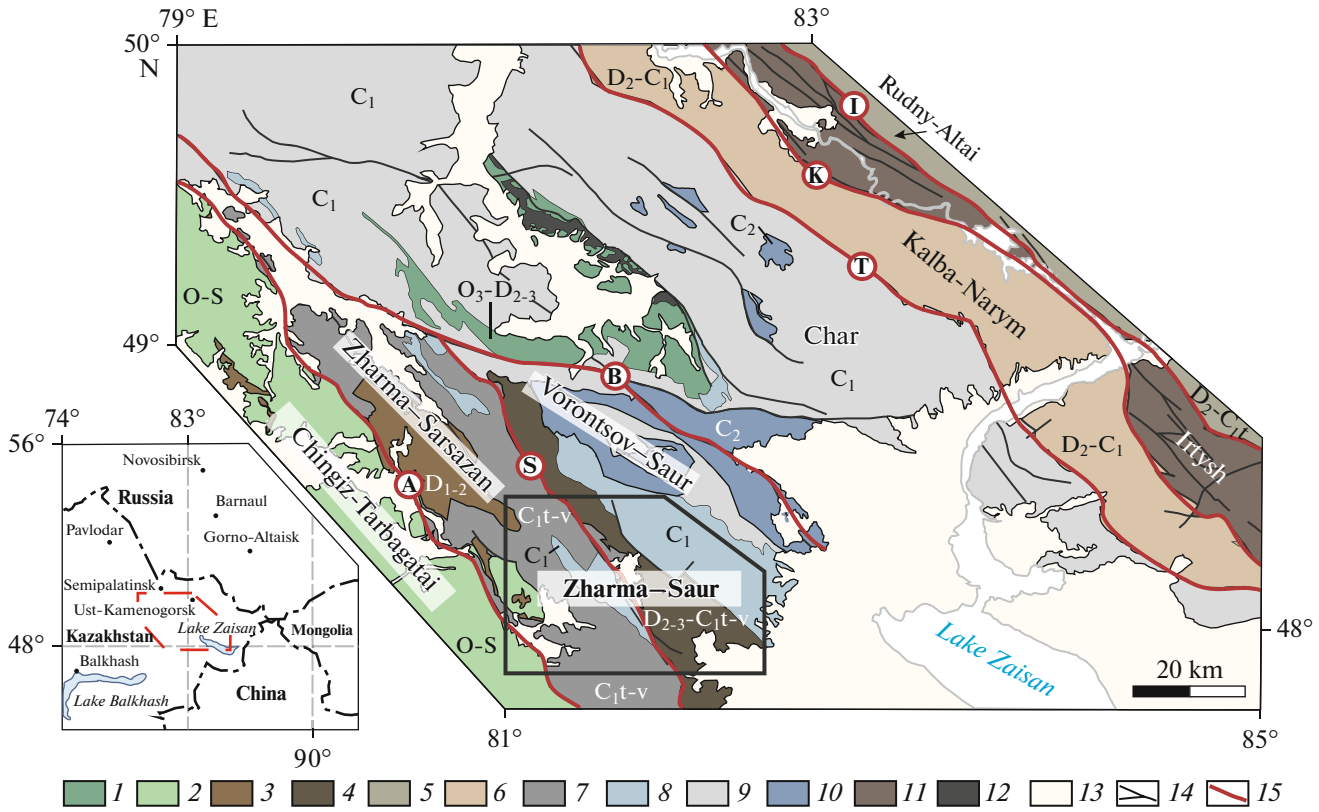

Fig. 1. Geological scheme of Ob'–Zaisan folded area (modified after [7, 24]). Inset shows geographical position of study area (polygon). *Large faults*: A, Arkalyk; S, Sirektas; B, Boko-Baiguzin; T, Terekta; K, Kalba-Narym; I, Irtysh. (*1–2*) Lower–Middle Paleozoic volcanogenic-sedimentary deposits in zones: (*1*) Char (O_3–D_{2-3}), (*2*) Chingiz-Tarbagatai (O–S); (*3*) Lower–Middle Devonian medium acid volcanic rocks (D_{1-2}); (*4–5*) Middle–Upper Paleozoic volcanogenic-sedimentary rocks in following zones: (*4*) Zharma-Saur (D_{2-3}–C_1t-v), (*5*) Rudny Altai (D_2–C_1t); (*6*) Devonian–Carboniferous sedimentary deposits of Kalba-Narym zone; (*7–8*) Lower Carboniferous volcanogenic-sedimentary rocks of Zharma-Saur island arc zone: (*7*) Kokon' and Sirektas Fm. (C_1t-v), (*8*) Koyanda and Tersairyk Fm. (C_1); (*9*) sedimentary deposits (C_1); (*10*) molasse (C_2); (*11*) mélange in Irtysh shear zone; (*12*) serpentinite mélange in Char zone; (*13*) Cenozoic deposits; (*14*) large faults; (*15*) structural boundaries of zones and subzones.

GEOLOGY

The formation of the CAOB is associated with the evolution and closure of the Paleo-Asian Ocean during the collision of the Siberian, Tarim, and North China cratons, numerous microcontinents and complexes of the different geodynamic nature [1, 10, 12, 16, 22, 30, 33, 40, 49, 63].

The formation of the northeastern part of the Kazakhstan Paleocontinent, also designated as the Boshchekul-Chingiz folded area, formed as a result of mutual accretion of a several of Cambrian-Ordovician island arcs of the Paleo-Asian ocean during the Silurian period. [6–9, 29, 41]. In the Late Paleozoic, the eastern margin of the Kazakhstan Paleocontinent (in modern coordinates) developed in the active continental margin, which led to the formation of the Devonian and Balkhash-Yili volcano-plutonic belts [18, 19, 28]. The evolution of the northeastern margin of the Kazakhstan Paleocontinent in the Devonian and Carboniferous periods, known as the Chingiz-Tarbagatai segment of the Boshchekul-Chingiz folded area (hereafter, Chingiz-Tarbagatai zone), is closely related to the development of the associated Zharma-Saur volcanic arc.

Currently, different geodynamic models of the formation and evolution of the structures of the Zharma-Saur island arc system have been developed, differing in the direction of the subduction plate and the parallel position of the volcanic arc relative to the Early Paleozoic complexes of the Kazakhstan Paleocontinent.

Based on the results of geological and geochemical studies of the rocks in the Zharma-Saur and Chingiz-Tarbagatai zones, located on the territory of China, in northwestern Junggar region, several geodynamic models have been proposed [34, 35, 60, 65]. These models suggest that the Zharma-Saur arc island zone is an intra-oceanic island arc terrane that formed in the Late Paleozoic, at a significant distance from the Chingiz-Tarbagatai zone. Subduction of oceanic lithosphere occurred in two directions (in modern coordinates): northward (beneath the Zharma-Saur island arc) and southward (beneath the Chingiz-Tarbagatai arc complexes).

According to other geodynamic models, the emplacement of the Zharma-Saur island arc occurred in the Late Devonian to Early Carboniferous period due to the subduction of the lithosphere of the Ob'-Zaisan oceanic basin beneath the northeastern margin of the Paleo-Kazakhstan continent, i.e., in a southward direction in modern coordinates [7, 11, 41, 58, 64].

In the works [11, 41], the Zharma-Saur island arc zone is considered an independent structure that drifted in the Paleo-Asian Ocean and was accreted to the Chingiz-Tarbagatai zone in the Carboniferous [38]. This suggests that the Zharma-Sarsazan subzone is a back-arc basin, formed as a result of subduction beneath the northeastern margin of the Kazakhstan Paleocontinent. The emplacement of the Zharma-Saur island arc zone occurred in close proximity to the compositional complexes or on the complexes of the Early Paleozoic island arcs of the Chingiz-Tarbagatai zone.

Another model is discussed in the works [7, 58, 64], which propose the development of the western part of the Zharma-Saur island arc zone (Zharma-Sarsazan subzone) is thought to represent the Carboniferous sedimentary basin that was emplaced on the Early Paleozoic basement of the Chingiz-Tarbagatai zone.

STRUCTURE OF THE ZHARMA-SAUR ISLAND ARC ZONE

The first information about the geology of this region was presented in the works of V.P. Nekhoroshev, D.S. Korzhinsky, V.N. Lodochnikov back in the early 1930s of the last century [13]. Since 1955, the first geological survey work began in this area, the results of which are presented in the work [20]. Subsequently, the main scientific interest of geologists studying the Zharma-Saur zone was associated with intrusive complexes, the so-called Zharma-Saur batholith, as well as with the accompanying deposits of rare earth metals [2, 13, 23, 48]. At the same time, detailed studies of volcanic and volcanogenic-sedimentary units of this zone, with the exception of geological survey work [17], were not carried out and ideas about their composition and age have practically not developed since the middle of the 20th century. However, all adjacent regions are characterized by a high level of study, taking into account precision analytical studies: the Early Paleozoic complexes of the Boshchekul-Chingiz folded area [7–9], formations of the eastern part of the Ob'-Zaisan folded area [3, 24, 56, 57], as well as part of the Zharma-Saur zone, localized in the territory of China [34, 35, 58, 60, 65].

The Zharma-Saur is a NW trending zone of volcanic and volcanogenic-sedimentary strata extending for >450 km (within eastern Kazakhstan and northwestern China) [13, 14, 17, 26, 32, 34, 63]. The Zharma-Saur zone is considered a paleo island arc system that formed within the Ob'-Zaisan branch of the Pale-Asian Ocean during Late Paleozoic [1, 7, 11, 21, 41, 56, 57] (Fig. 1). According to the geological structure and material composition of rocks, the Zharma-Saur zone can be divided into two subzones (Fig. 2): Zharma-Sarsazan in the west and Vorontsov-Saur in the east.

Zharma-Sarsazan Subzone

According to [4, 5, 7, 14, 17], the basement of the section in the Zharma-Sarsazan subzone is composed of basic-intermediate volcanics and tuffs of the Namas Fm. of the Lower Ordovician, as well as volcanics, sandstones and shales of the Donenzhal Fm. of Silurian age, unconformably overlying the Namas Fm. Structurally, above them, with unconformity, lie acidic volcanics of the Mashan Fm. of the Lower and Middle Devonian, and above them, with unconformity, lie basic volcanics of the Middle Devonian and red-colored terrigenous rocks of the Middle and Upper Devonian Givet-Frasnian Stages. The Lower Carboniferous sequence of the Lower Visean age are represented mainly by terrigenous rocks, unconformably overlying rocks of the Ordovician, Devonian and Silurian ages. Volcanic rocks and tuffs lie with angular unconformity on the Lower Visean rocks, and to a lesser extent, terrigenous rocks of the Sirektas Fm. of the Upper Visean – Lower Serpukhovian Stages [5, 14]. The Zharma-Sarsazan subzone is mainly composed of a thick (up to 2000 m) Lower Visean terrigenous sequence – the Kokon' Fm. This formation can be traced over a distance of more than 140 km as a NW trending. The Kokon' Fm. includes (Fig. 3) gravelstone, inequigranular polymictic sandstones, silty sandstones, clayey, siliceous-clayey, carbonaceous-clayey siltstones, calcareous sandstones with limestone lenses [4, 5]. The sequence of the formation is generally uniform and represents a multiple alternation of inequigranular rock units with the development of coarse-grained varieties in the lower part of the formation, which is replaced by finer deposits up the sequence. In the middle part of the formation there is a horizon of carbonate deposits, among which brachiopod was found, allowing us to assign the age of the formation to the Lower Visean Stage (C_1v) [5, 14, 17]. The selection of lithological samples and a sample of silty sandstones (see Fig. 3) for geochronological study was carried out from the upper part of the formation. The sedimentation environment may be associated with slope facies (turbidites) based on the development of a large volume of sandstones, silty sandstones and siltstones with obvious gradational layering, as well as with shallow-water – marine settings due to the small distribution of carbonate rocks.

Vorontsov-Saur Subzone

The Upper Paleozoic formations of the Vorontsov-Saur subzone (Fig. 1) overlie the rocks of the Zharma-Sarsazan subzone from the northeast.

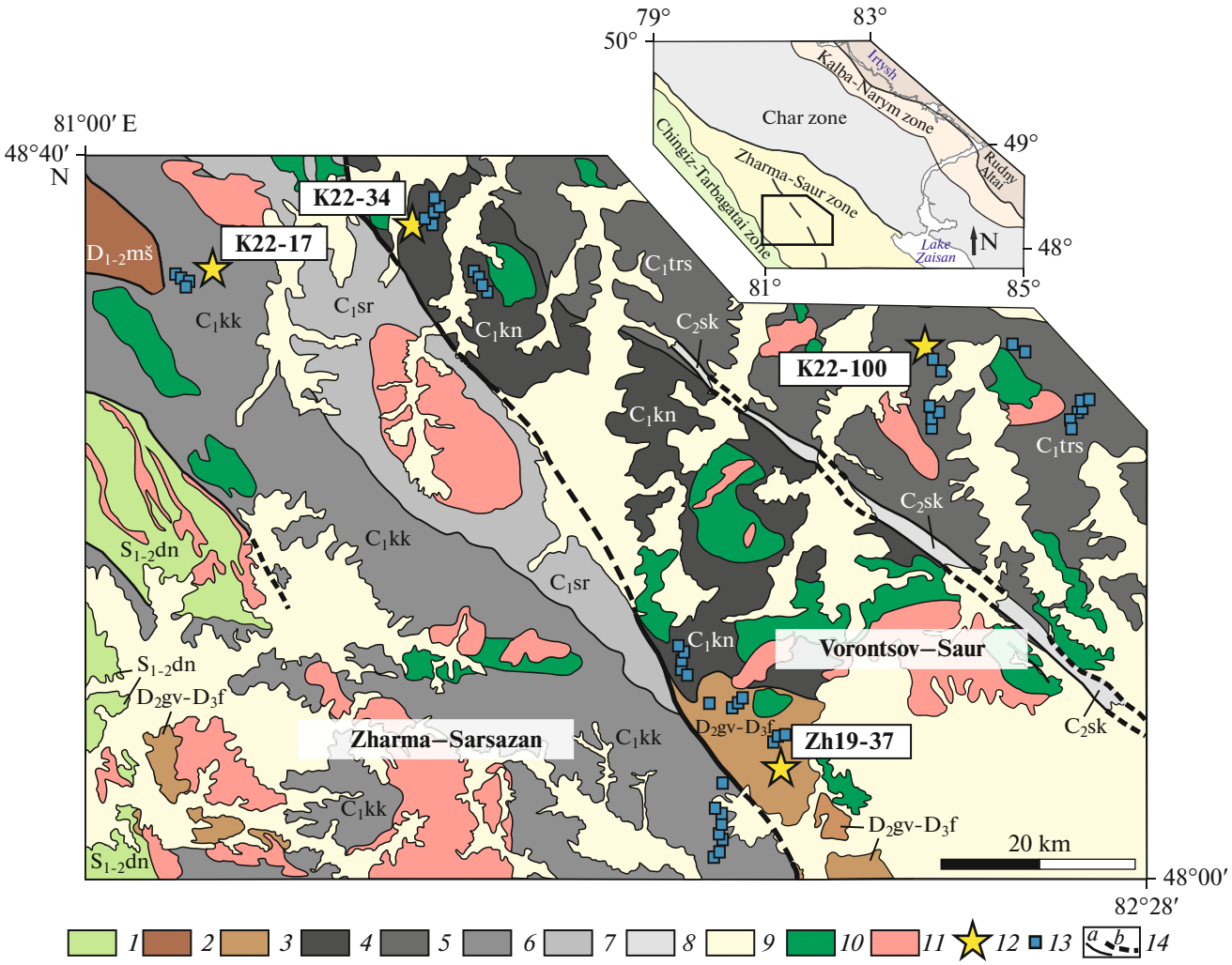

Fig. 2. Geological scheme of Zharma-Saur island arc zone (after [5]). Onset (rectangle) shows position of zone. (*1–8*) Formations and units: (*1*) Donenzhal Fm. (S_{1-2}dn), (*2*) Mashan Fm. (D_{1-2}mš), (*3*) Givetian–Frasnian unit (D_2gv–D_3f), (*4*) Koyanda Fm. (C_1kn), (*5*) Tersairyk Fm. (C_1trs), (*6*) Kokon' Fm. (C_1kk), (*7*) Sirektas Fm. (C_1sr), (*8*) Sarkul Fm. (C_2sk); (*9*) Cenozoic deposits; (*10–11*) intrusive complexes: (*10*) gabbroids, (*11*) granitoids; (*12*) samples for geochronological study; (*13*) lithological samples; (*14*) faults: (*a*) confirmed, (*b*) inferred.

Its structure includes volcanogenic-sedimentary (mainly) and sedimentary Devonian–Carboniferous stratified units.

The Givetian–Frasnian unit crops out in the southeast of the subzone, where it composes the main part (1200 m thick). The sequence includes inequigranular polymictic sandstones, gravelstone, as well as horizons of siltstones and conglomerates (Fig. 3). The basal part of the sedimentary sequence is composed of conglomerates, gravelstone, and coarse-grained sandstones with conglomerate lenses. Siltstones interbedded with the sandstones and gravelstone, are widely distributed in the upper part of the sequence. The age of the Givetian–Frasnian unit was estimated based on the finds of fossil flora, as well as brachiopod and bivalve fossil remains in the upper part of the section [4, 5, 14]. Samples were taken from the middle and upper parts of the Givetian–Frasnian unit; a sandstone sample (see Fig. 3) for geochronological study was taken from the roof of the unit.

The Middle–Upper Devonian formations overlie the Lower Carboniferous (Tournaisian) Koyanda Fm. sharply unconformably. The latter is widespread in the central part of the Vorontsov-Saur subzone to the southwest from the Sarkul Fault (Figs. 1, 2). The following rocks can be found in the Koyanda Fm.: basalts, basaltic andesites, andesites, tuffs and tuff sandstones, as well as horizons of cherts, clayey–siliceous and siliceous siltstones (Fig. 3). The formation includes the olistostrome facies, which is represented by boulders of siliceous and clayey-siliceous siltstones, as well as andesites, basalts, and tuffs scattered in the tuffaceous–terrigenous matrix. Tournaisian age of the Koyanda Fm. is conventionally accepted based on its

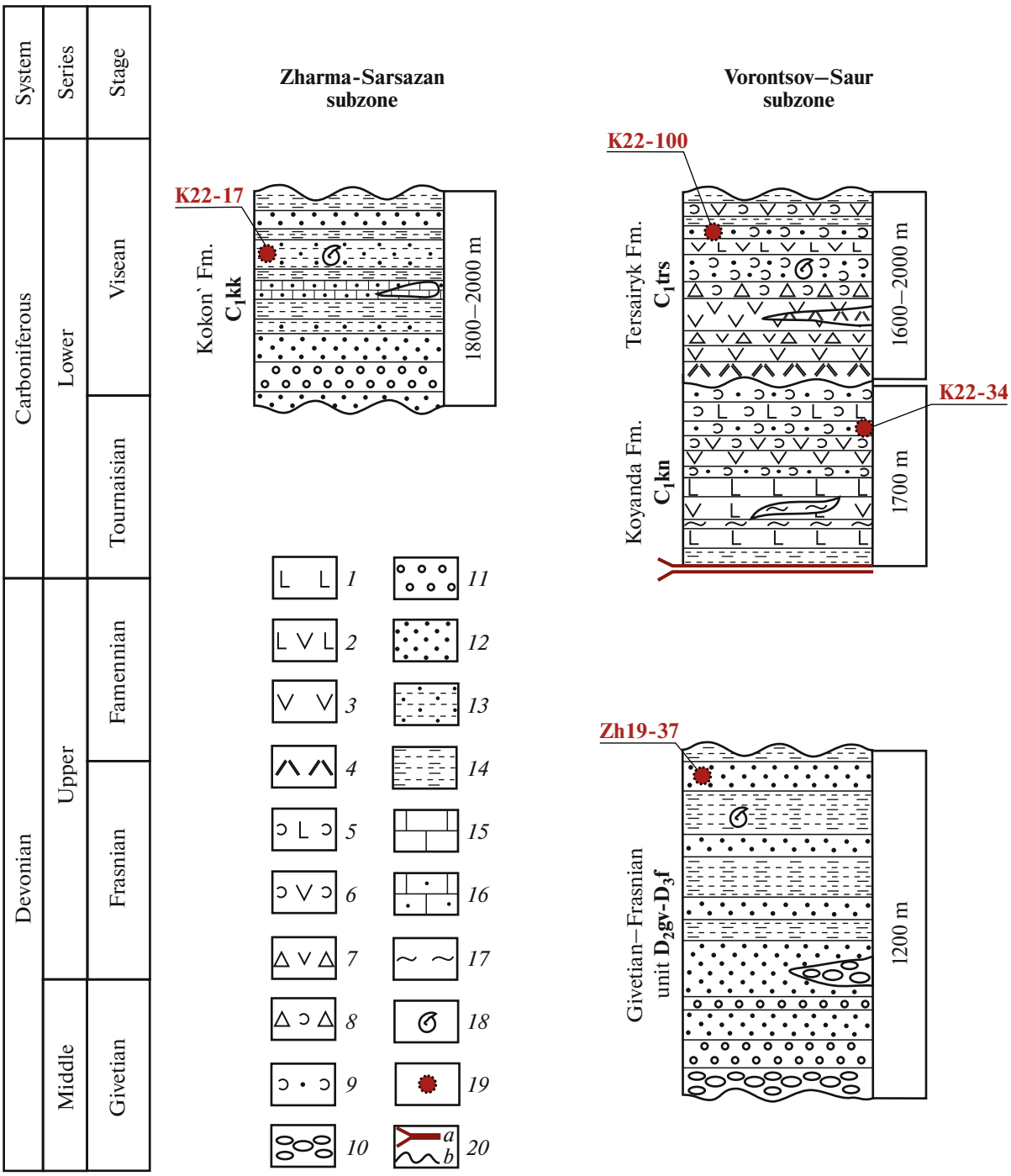

Fig. 3. Schematic lithological columns of up to the Middle Carboniferous of the studied stratigraphic units within the Zharma-Saur island arc zone (modified after [4, 5]). (*1*) Basalts; (*2*) basaltic andesites; (*3*) andesites, trachyandesites; (*4*) dacites; (*5*) basic tuffs; (*6*) medium acid tuffs; (*7*) lava breccias; (*8*) tuff breccias; (*9*) tuff sandstones; (*10*) conglomerates; (*11*) gravelstones; (*12*) sandstones; (*13*) silty sandstones; (*14*) siltstones; (*15*) limestones; (*16*) calcareous sandstones; (*17*) cherts; (*18*) fossils; (*19*) samples for isotope dating of detrital zircons; (*20*) contacts: (*a*) tectonic, (*b*) unconformable.

overlap by the Middle–Late Devonian sequences and the few determinations of the brachiopod fauna [5, 14, 17]. Thickness of the formation is 1700 m. During field work, lithological samples were collected from both the upper and lower parts of the formation, and a sample of tuff sandstones (Fig. 3) for geochronological study was taken from the upper part of the section.

Lower Visean Tersairyk Fm. is located northeast from the Sarkul Fault, which is marked by deposits of the Sarkul Fm. (C2) (Figs. 1, 2).

In the western part of the polygon, the Tersairyk Fm. unconformably overlies the volcanogenic-sedimentary Koyanda Fm. Outside the study area, the Tersairyk Fm. is overlain with angular unconformity by carbonate and terrigenous rocks of Upper Visean age. Frequent facies transitions of volcanics into volcanogenic-sedimentary and then into terrigenous rocks are distinguished in the structure of the formation. The Tersairyk Fm. is composed of medium and acidic volcanics, their lava breccias and tuffs, tuff sandstones, clayey and clayey-siliceous siltstones, and less common are basaltic andesites in the upper part of the section (Fig. 3). The age of the Tersairyk Fm. is considered Upper Tournaisian–Lower Visean based on the presence of brachiopod and crinoid fossils in tuff sandstone interbeds [4, 5, 14, 17]. Lithological samples were collected from all levels of the formation; a sample of tuff sandstones (Fig. 3) for geochronological study was confined to its upper part.

The intrusive magmatism within the Zharma-Saur zone, represented by the rocks of the Saur complex (330–315 Ma) and the Zharma-Saur batholith (305–275 Ma), is associated with the closure of the Ob'-Zaisan oceanic basin and post-orogenic magmatism.

The massifs composed of gabbro-diorite-granodiorites of the Saur complexes are widespread in the Zharma-Sarsazan and Vorontsov-Saur subzones. The zone of the Early Permian granitoids, a part of the Zharma-Saur batholith, extends for >400 km in the northwestern direction along the Zharma fault and is localized in the Zharma-Sarsazan subzone [13, 21, 46].

MATERIALS AND METHODS

U–Pb dating of detrital zircons was performed using a 193 nm Analyte Excite Excimer Laser Ablation System (Teledyne Cetac Technologies, Omaha, Nebraska, USA) equipped with an ICAP Qc mass spectrometer (Thermo Fisher Scientific, Bremen, Germany) in the Center for Geothermochronology at the Kazan Federal University (Kazan, Russia).

We performed all measurements by masses ^{202}Hg, ^{204}(Pb + Hg), ^{206}Pb, ^{207}Pb, ^{208}Pb, ^{232}Th, ^{235}U, ^{238}U. The laser beam diameter was 35 μm, pulse repetition rate was 5 Hz and laser energy density was 3.0 J/cm^2. Two standards (external and internal) were measured to analyze the sample.

We used international zircon reference samples:

— 91500 as a control sample (1065 Ma, [62]);

— Plešovice as an external standard (337 Ma, [59]).

The external standard was used to correct for elemental fractionation during laser ablation, mass discrimination, and drift of mass spectrometer settings over time. A control sample was measured to verify the correctness of the measurements.

NIST SRM 612 standard synthetic glass was additionally measured at the beginning, middle, and end of the measurement session to take mass spectrometer sensitivity into account. Mass spectrometric data processing, correction accounting, selection of the optimal signal area, as well as calculation of isotopic ratios (^{207}Pb/^{206}Pb, ^{206}Pb/^{238}U, ^{207}Pb/^{235}U, ^{208}Pb/^{232}Th) and corresponding ages were performed using the Iolite 3.65 software embedded in IgorPro 7 [54].

U–Pb isotope ratios were normalized to the corresponding isotopic ratios of standard zircon samples 91500 [62] and Plešovice [59]. The errors of single analyses (ratios, ages) and the calculated concordant ages are given at the 2σ level. Calculation of weighted average ages from isotopic ratios and construction of concordance diagrams were performed in Microsoft Excel using the Isoplot 4.15 software package [50].

The ^{206}Pb/^{238}U zircon ages younger than 1000 Ma, with discordance D (%) ranging from −10 to +10%, were used to construct the relative probability histogram.

Measurements with discordance of ≤10% or >10% were excluded from the sample. The formula used to calculate discordance is as follows:

$$D = 100 \times (\mathrm{Age}(^{207}\mathrm{Pb}/^{235}\mathrm{U}) / \mathrm{Age}(^{206}\mathrm{Pb}/^{238}\mathrm{U}) - 1).$$

Estimation of the Maximum Depositional Age (MDA) was carried out by calculating the weighted average age of the population of the youngest zircons, overlapping within 2σ [38].

The petrographic study involved quantitative counting of grains (mineral composition counting) in the rocks, carried out by direct measurement of rock fragments arranged along a straight line in the field of a microscope. Medium-grained sandstones with 0.20–0.50 mm grains were selected for counting. Measurements were taken using a scale bar in the eyepiece of the microscope (0.04 mm for Axio Scope A1, Carl Zeiss AG, Oberkochen, Germany).

For each sample (n = 21), 250–300 grains were counted, which were determined as:

— mono- and polycrystalline quartz (Qm and Qp, respectively);

— plagioclase (Pl);

— potassium feldspar (Kfs);

— fragments of volcanic (Lv) and sedimentary (Ls) rocks;

— matrix (M).

The data obtained were then converted into quantitative percentages. Based on these data, classification and discriminant triangle diagrams were constructed.

Determination of the contents of the main rock-forming elements was performed by X-ray fluorescence analysis (XRF) in the Center for Collective Use for Multielemental and Isotope Studies at the Institute of Geochemistry and Geophysics of the Siberian

Table 1. Characteristics of geochronological samples of sandstones and tuff sandstones of Zharma-Saur island arc zone and U–Pb ages obtained

Sample	Unit/Fm.	Rock	Coordinates	*N*	Age, Ma	MDA, Ma
Zh19-37	Givetian–Frasnian	Sandstone	48°08′05.40″ N 81°54′22.70″ E	78	498, 451, 423, 401	392 ± 4
K22-34	Koyanda	Tuff sandstone	48°34′57.68″ N 81°28′59.01″ E	64	348	345 ± 2
K22-100	Tersairyk	Tuff sandstone	48°28′46.17″ N 82°17′23.65″ E	38	355	353 ± 2
K22-17	Kokon’	Silty sandstone	48°37′53.96″ N 81°02′19.34″ E	92	518, 429, 352	352 ± 2

N—number of grains with concordant ages within limits of ±10%; MDA—maximum deposition age.

Branch of the Russian Academy of Sciences (Novosibirsk, Russia) following the technique [15]. The measurements were performed on an ARL-9900XP X-ray fluorescence spectrometer (Thermo Fisher Scientific, Bremen, Germany). When constructing classification and discriminant diagrams, the concentrations of rock-forming oxides were converted to dry residue (LOI was excluded).

The inductively coupled plasma mass spectrometry (ICP-MS) was applied to measure contents of rare earth (La, Ce, Pr, Nd, Sm, Eu, Gd, Tb, Dy, Ho, Er, Tm, Yb, Lu) and trace (Rb, Sr, Cs, Ba, Nb, Zr, Y, Hf, Ta, Th, U) elements using a Finnigan Element II single-collector mass spectrometer (Thermo Fisher Scientific, Bremen, Germany) at the CCU MIS IGM SB RAS (Novosibirsk, Russia; analyst I.V. Nikolaeva). The powders were processed according to the Jenner Protocol [47]. The BHVO-1, BCR-1, and JB-3 international standards [53] were used to evaluate the accuracy/inaccuracy of measurements. Analytical errors were 2–7% for REE and HFSE.

Determinations of Nd concentrations and isotopic composition were carried out at the CCU “Geoanalytik” (IGG Ural RAS, Ekaterinburg, Russia).

The procedure for chemical preparation of the samples involved the decomposition of the samples with a mixture of mineral acids at 120°C, followed by the addition of an isotopic spike of ^{149}Sm–^{150}Nd, chromatographic REE separation, and stepwise separation of Sm and Nd.

Isotopic ratios were measured by TIMS on a Triton Plus spectrometer (Thermo Fisher Scientific, Bremen, Germany) in static mode.

The measurement validation was performed using the isotopic standard JNd_i-1 (GSJ). During operation, the $^{143}Nd/^{144}Nd$ ratio in the standard was 0.512111 ± 9 (2 SD, $n = 7$).

RESULTS

U–Pb Dating of Detrital Zircons

U–Pb dating of detrital zircon grains has been carried out for sedimentary and volcanogenic-sedimentary rocks from the Zharma-Saur island arc zone (Fig. 2; Table 1; Supplement 1 (Table P1).

Samples were collected from:

— Givetian–Frasnian unit (Zh19-37, sandstone);

— Koyanda Fm. (K22-34, tuff sandstone);

— Tersairyk Fm. (K22-100, tuff sandstone);

— Kokon’ Fm. (K22-17, silty sandstone).

In the analyzed samples, zircons are small to medium in size (40 to 180 microns), transparent, colorless, occasionally with a yellowish tint. The grains are non-rounded and have predominantly prismatic, less often isometric shape.

Zircons are characterized by fine oscillatory zoning and a Th/U ratio between 0.21 and 2.15, confirming their magmatic origin (Figs. 4a, 4b, Supplement 1 (Table P1)).

Givetian–Frasnian Unit. A total of 96 zircon grains were analyzed from the Zh 19–37 sandstone sample of the Givetian–Frasnian unit, 18 of which were excluded due to discordance of the obtained. The age interval for 78 grains varies from 378 ± 12 to 521 ± 15 Ma. Four age groups are distinguished on the histogram (Fig. 5a): (1) Devonian 415–378 Ma ($n = 26$) with a peak at 401 Ma; (2) Silurian 440–419 Ma ($n = 22$) with the main peak at 432 Ma; (3) Ordovician 476–446 Ma ($n = 25$) with a peak at 451 Ma; (4) Late Cambrian 492 – 502 Ma ($n = 3$) with a peak at 498 Ma. Single grains not included in age groups have ages of 518 ± 12 and 521 ± 15 Ma. The weighted average age of the youngest zircons corresponds to 392 ± 4 Ma ($n = 17$) (Fig. 5e), and the age of the youngest peak is 401 Ma.

Koyanda Fm. From sample K22-34 of the tuffaceous sandstone of the Koyanda Fm., 90 zircon grains were analyzed. Of these, 26 grains were not considered due to their discordant values.

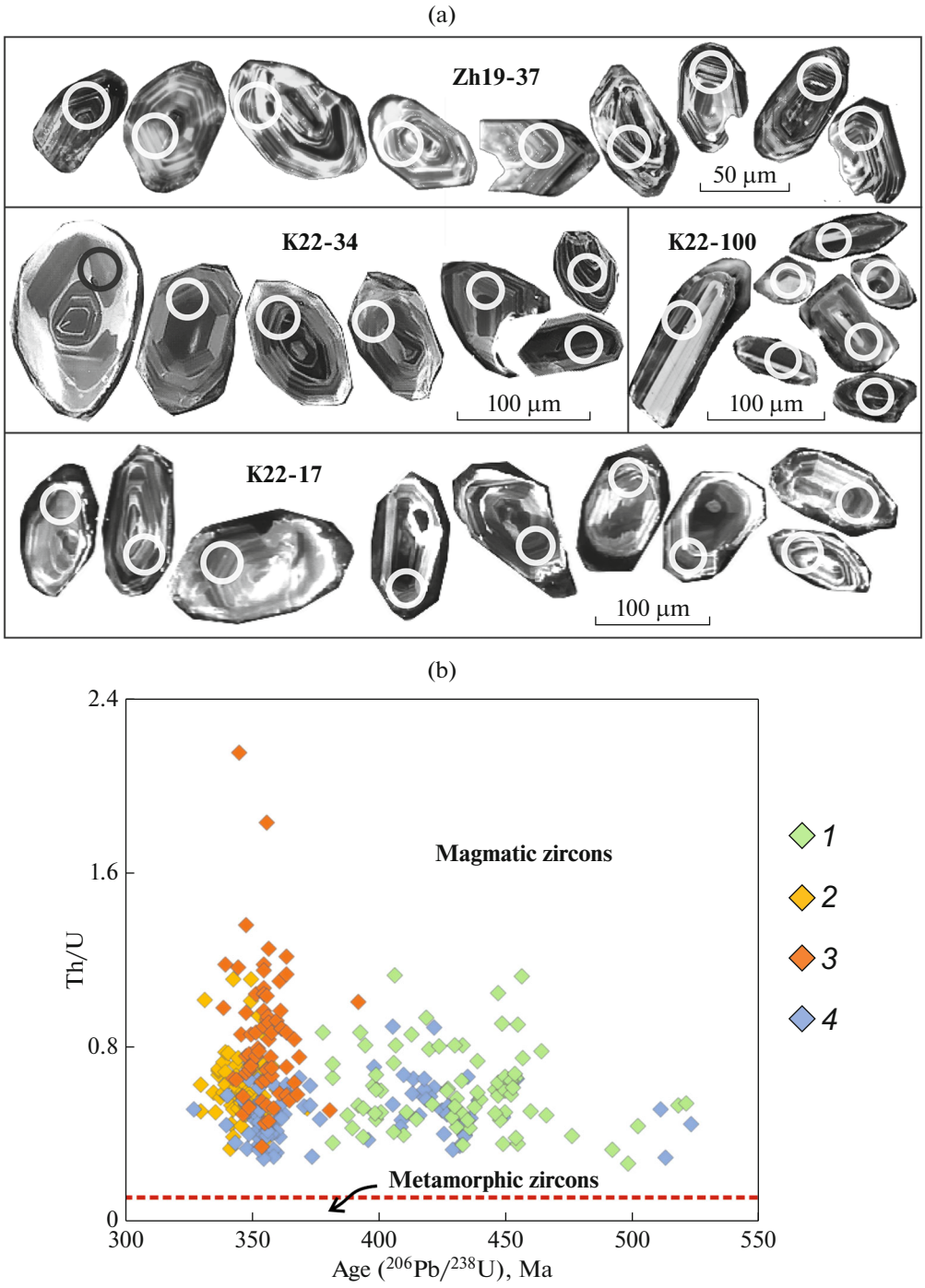

Fig. 4. (a) CL images of detrital zircons; (b) Th/U–Age plot. (*1*) Givetian–Frasnian unit (sample Zh19-37); (*2–4*) formations: (*2*) Koyanda (sample K22-34), (*3*) Tersairyk (sample K22-100), (*4*) Kokon' (sample K22-17)

The histogram for 64 grains establishes an age range from 384 ± 20 to 330 ± 13 Ma. The relative probability curve records the unimodal distribution of the age group 372–330 Ma (n = 63) with a peak at 348 Ma corresponding to the Tournaisian age (Fig. 5b). The age of a single grain coincides with the oldest zircon and corresponds to 384 ± 20 Ma. The age of the peak and the average age of the youngest zircon grains (Fig. 5f) are 348 and 345 ± 2 Ma (n = 57), respectively.

Tersairyk Fm. From the tuff sandstone sample K22-100, 72 zircon grains were analyzed. However, 34 of these grains were excluded from the consideration due to their discordant values. The age interval for 38 zircon grains varies from 392 ± 7 to 339 ± 22 Ma. The

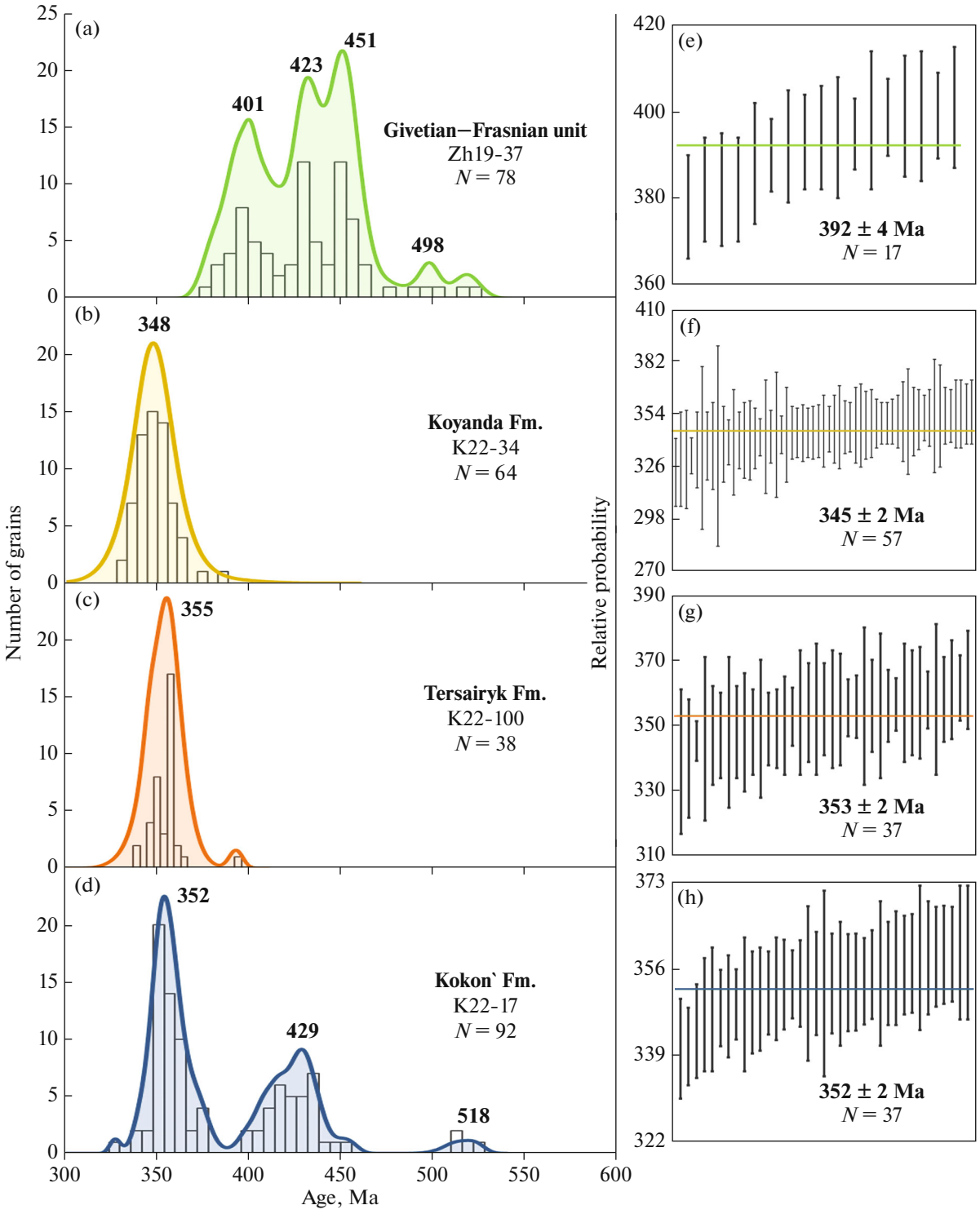

Fig. 5. Histograms and a relative probability curve for $_{206}Pb/_{238}U$ ages of detrital zircons with discordance of less than 10%, and weighted average age of youngest zircon population. (a)–(d) Histograms with a relative probability curve: (a) Zh19-37 (sandstones of Givetian–Frasnian unit); (b) K22-34 (tuff sandstone of Koyanda Fm.); (c) K22-100 (tuff sandstones of Tersairyk Fm.); (d) K22-17 (silty sandstone of Kokon' Fm.). (d)–(z) Diagrams with weighted average age: (d) Zh 19-37 (sandstone of Givetian–Frasnian unit), (e) K22-34 (tuff sandstone of Koyanda Fm.), (f) K22-100 (tuff sandstone of Tersairyk Fm.), (z) K22-17 (silty sandstone of Kokon' Fm.).

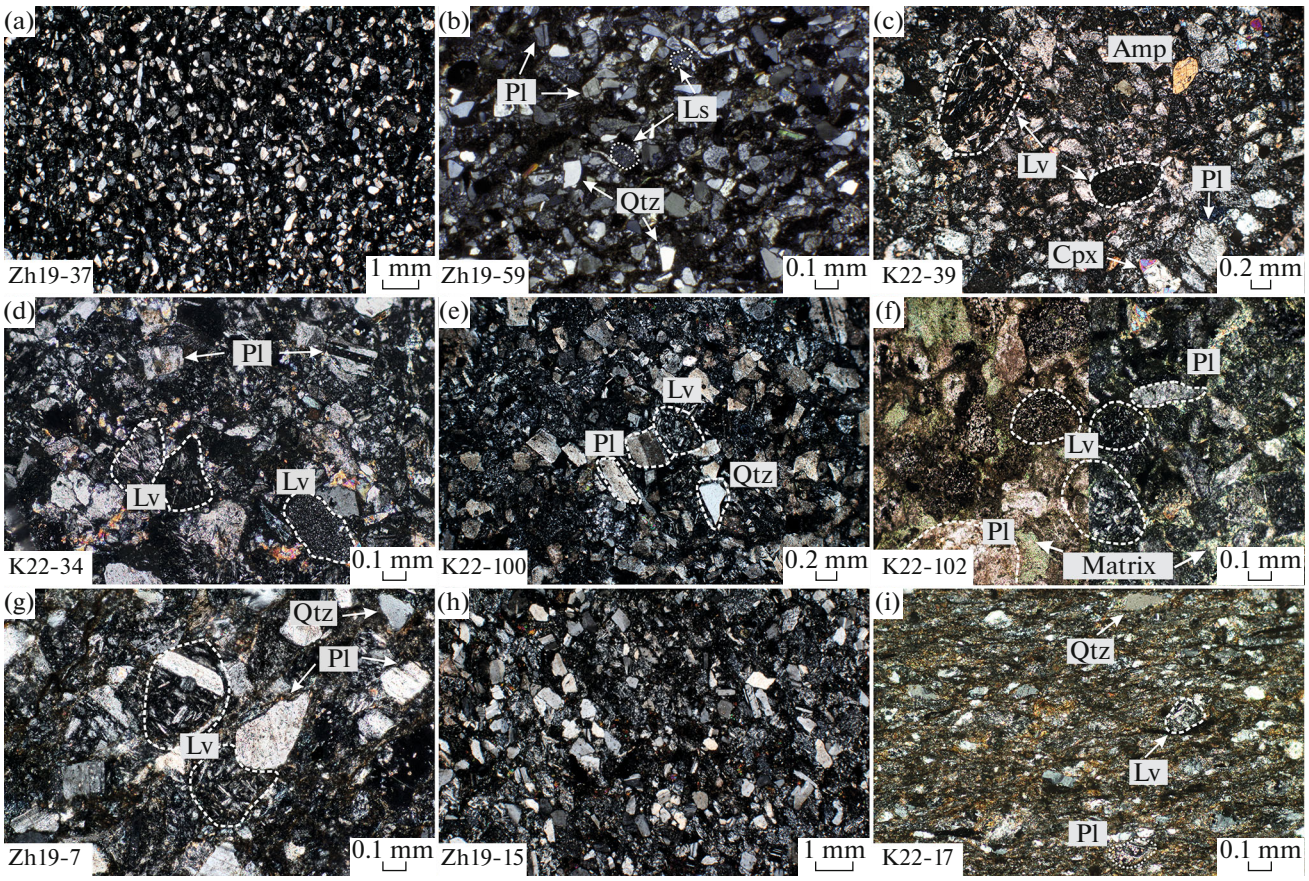

Fig. 6. Images of rock thin sections (crossed nicols), showing mineral composition and textural features of rocks. Notation: Qtz, quartz; Pl, plagioclase; Lv, fragments of volcanic rocks; Ls, fragments of sedimentary rocks; Amp, amphibole; Cpx, clinopyroxene. (a)–(b) Sandstones of Givetian–Frasnian unit; (c)–(d) tuff sandstones of Koyanda Fm.; (e)–(f) tuff sandstones of Tersairyk Fm.; (g)–(i) sandstones and silty sandstones of Kokon' Fm.

distribution of the age group 364–339 ($n = 37$) Ma has a unimodal character on the histogram with a peak at 355 Ma (Fig. 5c). The age of a single grain is the oldest zircon, corresponding to 392 ± 7 Ma. The age of the peak and the average age for the youngest zircon grains (Fig. 5c) coincide within the error limits and are 355 and 353 ± 2 Ma ($n = 37$), respectively, which allows us to determine the maximum age of deposition as Tournaisian (Fig. 5g).

Kokon' Fm. We have also analyzed 100 zircon grains from silty sandstone (sample K22-17) of the Kokon' Fm. Of these, 8 grains were excluded because of the discordance of the age values obtained.

The ages of 92 zircon grains on the histogram vary from 327 ± 6 to 523 ± 10 Ma. The relative probability curve fixes three age groups (Fig. 5d): (1) Early Carboniferous–Late Devonian 340–377 Ma ($n = 54$) with a single peak at 352 Ma; (2) Early Devonian–Silurian–Ordovician 396–455 Ma ($n = 34$) with a peak at 429 Ma; (3) Cambrian 511–523 Ma ($n = 3$) with a peak at 518 Ma. The age of a single grain is the youngest zircon, corresponding to 327 ± 6 Ma. The average age of the youngest zircon grains and the age of the youngest peak are 352 and 352 ± 2 Ma ($n = 37$), respectively, and their coincidence allows us to determine the maximum age of deposition as Tournaisian (Fig. 5h).

PETROGRAPHY

In the Givetian–Frasnian unit, we studied gray-green fine- to medium-grained sandstones with psammitic texture and massive structure (Figs. 6a, 6b).

The clastic framework of the rocks is represented by: subrounded to non-rounded grains of plagioclase (34–44%) and volcanic rocks (19–32%); fragments of siliceous sedimentary rocks (5–14%) are less common.

The total content of monocrystalline and polycrystalline quartz ranges from 18 to 28%. The degree of sorting of clastic materials is predominantly medium. The matrix type in the sandstones is contact, and its content averages 4% of the rock volume. Accessory minerals are zircon, apatite, and rutile. To classify the rocks, we used Folk's [43, 44] and Shutov's [25] triangular diagrams, on which the data points, converted into percentages of rock components, were plotted (see Suppl. 1 (Table P2)).

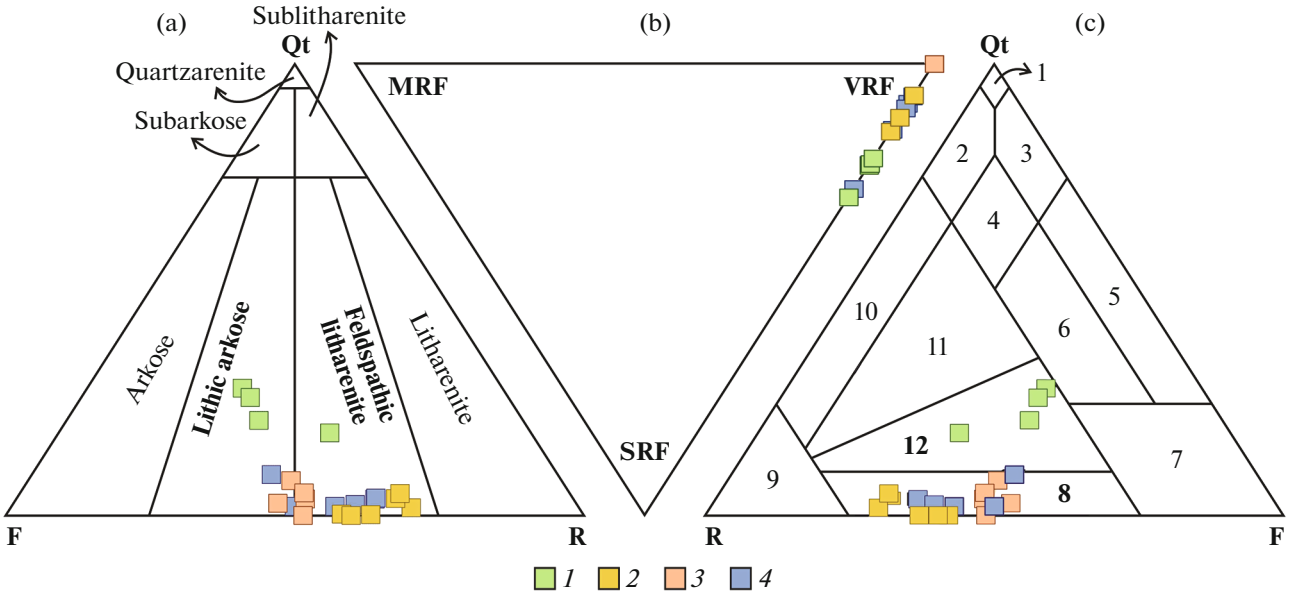

Fig. 7. Classification diagrams for sandstones. (a)–(b) after [43, 44]; (c) after [25]. Designations: Qt—sum of polycrystalline and monocrystalline quartz; F, total feldspars; R, total volcanic and sedimentary rock fragments. Rock fragments: MRF, metamorphic, VRF, volcanic; SRF, sedimentary. Arabic numerals: (1–4) sandstones: (1) monomictic quartz, (2) silicoclastite–quartz, (3) feldspar–quartz, (4) mesomictic quartz; (5) arkoses; (6) greywacke arkoses; (7) field of nonterrigenous rocks; (8) feldspar greywackes; (9–12) greywackes: (9) greywackes, (10) quartz, (11) feldspar-quartz, (12) quartz-feldspar. (*1*) Sandstones of Givetian–Frasnian unit (D_2gv–D_3f); (*2–4*) sandstones of formations: (*2*) Koyanda (C_1kn) (tuff), (*3*) Tersairyk (C_1trs) (tuff), (*4*) Kokon' (C_1kk).

The sandstones correspond to lithic arkoses, according to the classification of [43] (Fig. 7a), and quartz-feldspar graywackes, according to [25] (Fig. 7c).

The Givetian–Frasnian sandstones are characterized by a higher proportion of fragments of sedimentary rock compared to the sandstones from other studied formations (Fig. 7b).

The fine- to medium-grained tuff sandstones, rarely coarse-grained, with a psammitic texture and a massive structure, are considered in the Koyanda Fm. (Figs. 6c and 6d).

The clastic framework of the rocks (Fig. 6c) is represented by plagioclase grains (33–47%) and fragments of volcanic (44–62%) and sedimentary (up to 9%) rocks, plagioclase grains (33–47%), and fragments of volcanic (44–62%) and sedimentary (up to 9%) rocks. Fragments of brown amphibole and clinopyroxene crystals are rare (Fig. 6c).

The total quartz content in the tuff sandstones is very low, sometimes reaching only 5%. The degree of sorting of the clastic material is also low. According to the degree of roundness, the rock fragments are unrounded. There are also clastic grains with melted boundaries and jagged edges, indicating that the introduced volcanic component.

The matrix averages 3% of the total rock volume and is composed of mica-chlorite material. This matrix is of hydrochemical origin. Apatite occurs among the accessory minerals; the rock fragments are predominantly volcanic in composition (Fig. 7b).

In petrographic composition, the tuff sandstone corresponds to feldspathic litharenite according to classification [43], as shown in Fig. 7a. According to the classification of [25], it corresponds to feldspathic graywacke (Fig. 7c).

Tuff sandstones of the Tersairyk Fm. are fine- to coarse-grained, light to dark green (Figs. 6e, 6f).

The rocks have a psammitic texture and a massive, less frequently banded structure. They are composed of: plagioclase (40–50%) and fragments of volcanic rocks (39–48%); less commonly, there are fragments of amphibole, clinopyroxene (0–8%), and monocrystalline quartz (0–7%) crystals.

The degree of sorting is low to medium; the clasts are subangular. The proportion of the mica–chlorite matrix in the sample is 3–4%, on average.

According to classification [43], sandstones belong to feldspathic litharenites in terms of the composition of the main clastic components. According to the classification [25], they are classified as feldspathic graywackes (Figs. 7a, 7c).

On the composition diagram of the rock clasts, samples from the Tersairyk Fm. show the highest proportion of the volcanic material compared to rocks from other stratigraphic units (see Fig. 7b).

The sandstones of the Kokon' Fm. are mostly fine- to medium-grained, while silty sandstones are also present (Figs. 6g–6i).

The rocks are gray-green in color and have psammitic, less frequently aleuritic-psammitic texture and massive structure. The clastic framework of the rocks is represented by volcanic rocks (34–54%), plagioclases (33–46%), and less commonly sedimentary rock fragments (3–17%).

Some fragments of volcanic rocks have porphyritic, microlithic, and interstitial texture (Fig. 6g). The sandstones of the Kokon' Fm. have a low proportion of quartz, ranging from 2 to 9%.

The matrix averages 5% of the entire rock and is composed of a mixture of chlorite, epidote, xenomorphic plagioclase, and quartz. Based on the classification [43], these sandstones are classified as feldspathic litharenites (Fig. 7a), while according to the classification [25], they belong to feldspathic graywackes (Fig. 7c).

Rock clasts in sandstones are predominantly presented by volcanics (Fig. 7b).

The silty sandstone has a different mineral composition. It is intensively cataclased with the formation of a muscovite–biotite fine-grained aggregate between the grains of the rock framework. Quartz, plagioclase, and potassium feldspar, as well as small amounts of volcanic and sedimentary rocks were found among the clasts.

The degree of sorting of clastic material in the sedimentary rocks of the Kokon' Fm. is low; more rarely, medium. The degree of roundness of clasts ranges from unrounded to subangular. Accessory minerals are represented by zircon, apatite, and titanite.

The types of secondary alteration observed in all studied rocks are saussuritization and sericitization, and less frequently, pelitization of feldspar clastic grains. In addition, the volcanic rock clasts, unstable to weathering, are altered. This results in the subsequent formation of chlorite, epidote, ore minerals, and iron oxides.

PETRO-GEOCHEMICAL COMPOSITION OF SANDSTONES AND TUFF SANDSTONES

The contents of major rock-forming oxides were measured in 29 samples from the studied sections, and trace elements were measured in 24 samples. Data for ten samples were taken from [57] (Supplement 1: Tables P3, P4).

The SiO_2 content in sandstones is as follows (average–av.):

— 58.5–69.9 wt % (av. 63.4 wt %) Givetian–Frasnian unit;

— 52.2–64.4 wt % (av. 56.6 wt %) Koyanda Fm.;

— 51.7–57.3 wt % (av. 54.2 wt %) Tersairyk Fm.

The SiO_2 content in sandstones of the Givetian–Frasnian unit is higher than in rocks of the Koyanda and Tersairyk Formations.

Sandstones of the Kokon' Fm. have a SiO_2 content that varies between 57.2 and 64.9 wt %, occupying an intermediate position among the considered rocks (av. 60.1 wt %).

The average (av.) contents of Fe_2O_{3tot} and TiO_2 in sandstones:

— Fe_2O_{3tot} – av. 9.3 wt %, TiO_2 – av. 1.0 wt % (Givetian–Frasnian unit);

— Fe_2O_{3tot}–av. 7.3 wt %, TiO_2–av. 0.8 wt % (Koyanda Fm.);

— Fe_2O_{3tot}–av. 7.9 wt %, TiO_2–av. 0.9 wt % (Tersairyk Fm.);

— Fe_2O_{3tot}–av. 6.1 wt %, TiO_2–av. 0.8 wt % (Kokon' Fm.).

The average Fe_2O_{3tot} content in sandstones of the Givetian–Frasnian unit is higher than in sandstones of the Koyanda, Tersairyk, and Kokon formations.

A high MgO content is noted in tuff sandstones of the Tersairyk Fm.—from 2.9 to 5.5 wt % (av. 3.8 wt %), as well as in samples of the Koyanda Fm.—from 1.4 to 3.3 wt % (av. 2.4 wt %), which may be associated with the presence of a large volume of mafic volcanic material.

In the $\log(SiO_2/Al_2O_3)$–$\log(Na_2O/K_2O)$ diagram [55], plotted based on rock-forming oxide ratios, almost all data points of sandstones are distributed in the graywacke field (Fig. 8a). Low SiO_2/Al_2O_3 ratios indicate a low degree of rock maturity, suggesting that the sandstone is depleted in quartz and is dominated by aluminosilicates or clay mineral components. Higher Na_2O/K_2O ratios indicate the predominance of sodium feldspars over potassium feldspars and potassium mica. In the classification diagram used to separate graywacke and arkose, all the data points are located in the graywacke field. The only exception is a single point of silty sandstone from the Kokon' Fm., which falls within the arkose field, as confirmed by petrographic analysis [55] (Fig. 8b).

We applied the lithochemical classification of sandstones to obtain reliable information about the composition of the source rocks in the provenance area and degree of their weathering, the petrogenic or lithogenic nature of the sediments, as well as to obtain more accurate paleoreconstructions of tectonic conditions and sedimentation environments [27].

Values of hydrolyzate modulus (HM) [27],

$$HM = (Al_2O_3 + TiO_2 + Fe_2O_3 + FeO + MnO)/SiO_2 \quad (2)$$

range from 0.29 to 0.55. These values allow us to classify the sandstones under study as sialites.

Some rocks of the Koyanda Fm. and tuff sandstones of the Tersairyk Fm. have MgO levels greater than 3 wt %. This allows us to classify them as pseudosialites, which contain pyroclastic or volcanic

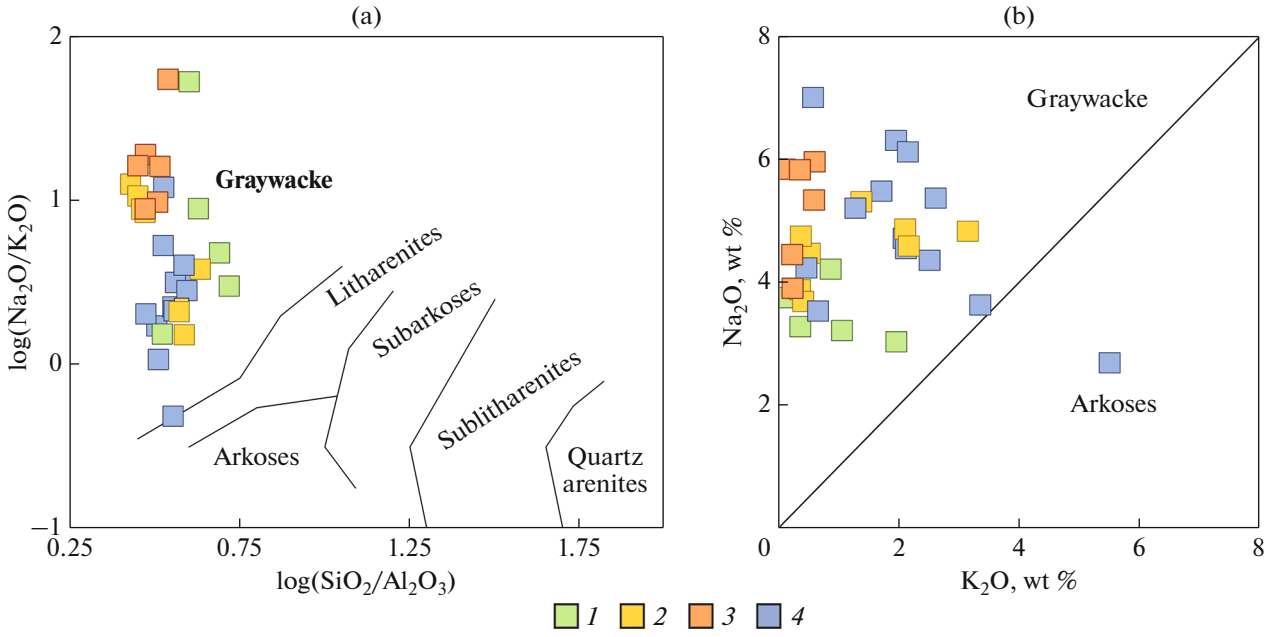

Fig. 8. Classification diagrams for sandstones (after [55]). (a) $\log(Na_2O/K_2O)$–$\log(SiO_2/Al_2O_3)$ diagram for sedimentary rocks; (b) diagram of separation of arkose and greywacke sandstones. (*1*) Sandstones of Givetian–Frasnian unit (D_2gv–D_3f); (*2*) tuff sandstones of Koyanda Fm. (C_1kn); (*3*) tuff sandstones of Tersairyk Fm. (C_1trs); (*4*) sandstones of Kokon' Fm. (C_1kk).

material [27]. In addition, we have calculated ferruginous (FM), titanium (TM), and normalized alkalinity (NAM) petrochemical modules. Based on the obtained correlation values (n = 29, with a critical value of the Pearson correlation coefficient of $r_c = 0.37$ at a 5% significance level) of the TM-FM (r = 0.83) and NAM-HM (r = –0.70), sandstones from the Kokon' and Koyanda formations, as well as the Givetian–Frasnian sequence, can be classified as rock-forming sedimentary rocks [27] (Fig. 9a). This allows us to classify them as pseudosialites, which contain pyroclastic or volcanic material [27]. In addition, we have calculated ferruginous (FM), titanium (TM), and normalized alkalinity (NAM) petrochemical modules. Based on the obtained correlation values (n = 29, with a critical value of the Pearson correlation coefficient of r_c = 0.37 at a 5% significance level) of the TM-FM (r = 0.83) and NAM-HM (r = –0.70), sandstones from the Kokon' and Koyanda formations, as well as the Givetian–Frasnian sequence, can be classified as rock-forming sedimentary rocks (Fig. 9a).

Based on the above characteristics, one can suggest that the chemical composition of the sandstones under consideration is similar to that of original igneous rocks.

The following petrochemical indices were used to determine the degree of chemical alteration of rocks in the provenance area:

— CIA, Chemical Index of Alteration [52];

— ICV, Index of Compositional Variability [36].

The CIA, which is calculated from the molecular amounts of petrogenic oxides using the formula:

$$\mathrm{CIA} = \left[Al_2O_3/(Al_2O_3 + CaO + Na_2O + K_2O)\right]\times 100 \quad (3)$$

is used as an indicator of the ratio of Al_2O_3 and chemically active oxides in the sample, reflecting the maturity (transformation into clay minerals) of the sediment.

The CIA value of 70 is used to differentiate between sediments formed under strong (CIA > 70) and weak (CIA < 70) weathering conditions. In the rocks studied, the CIA ranges from 41.04 to 69.05 (the zone of weak weathering), indicating a low degree of chemical weathering of the source rocks from the province (Fig. 9b).

Note that sandstones from the Givetian–Frasnian unit are characterized by higher CIA values (57.57–69.05) compared to sandstones from the Koyanda, Tersairyk, and Kokon formations. This may indicate the presence of more altered rocks in the provenance area.

The ICV is calculated using molecular quantities in accordance with the following formula:

$$\mathrm{ICV} = [(Fe_2O_3 + Na_2O + K_2O + CaO + MgO + TiO_2/Al_2O_3]. \quad (4)$$

This index is used to determine the maturity of rocks in the provenance area.

An value of ICV > 1 indicates immature source sediments with high contents of nonclay silicate minerals such as plagioclase, potassium feldspar, amphibole, pyroxene, and rock fragments. In contrast, more

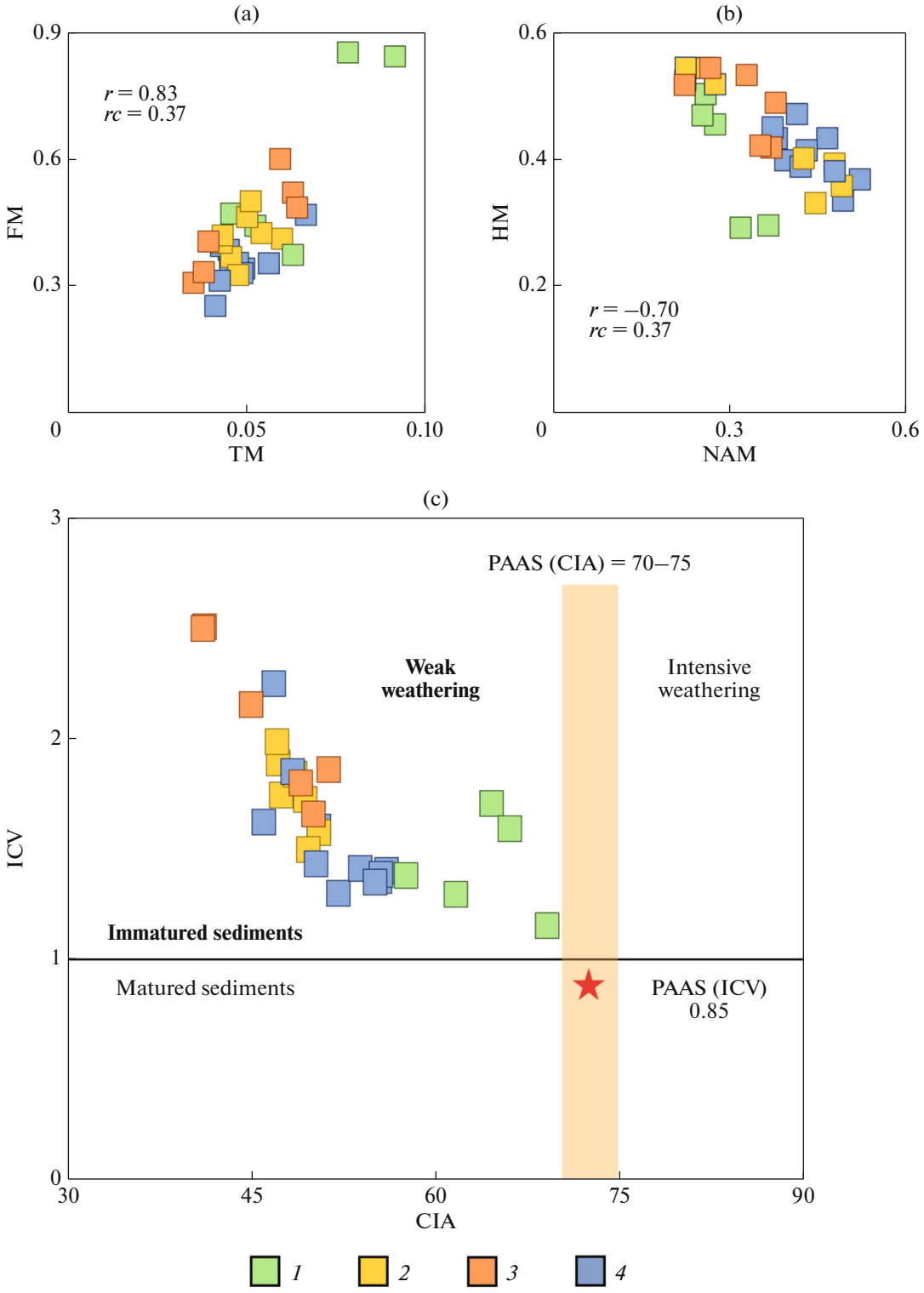

Fig. 9. (a) TM–FM and NAM–GM diagrams, after [27]; (b) diagram illustrating ratio between ICV (index of composition variability) according to [36] and CIA (chemical index of alteration) according to [52]. Notation: moduli: FM, femic; TM, titanium; HM, hydrolysate; and NAM, normalized alkalinity; r is correlation coefficient and r_c is critical value of Pearson's correlation coefficient. PAAS values are given after [61]. (*1*) Sandstones of Givetian–Frasnian unit (D_2gv-D_3f); (*2–3*) sandstones of formations: (*2*) Koyanda (C_1kn) (tuff), (*3*) Tersairyk (C_1trs) (tuff), (*4*) Kokon' (C_1kk).

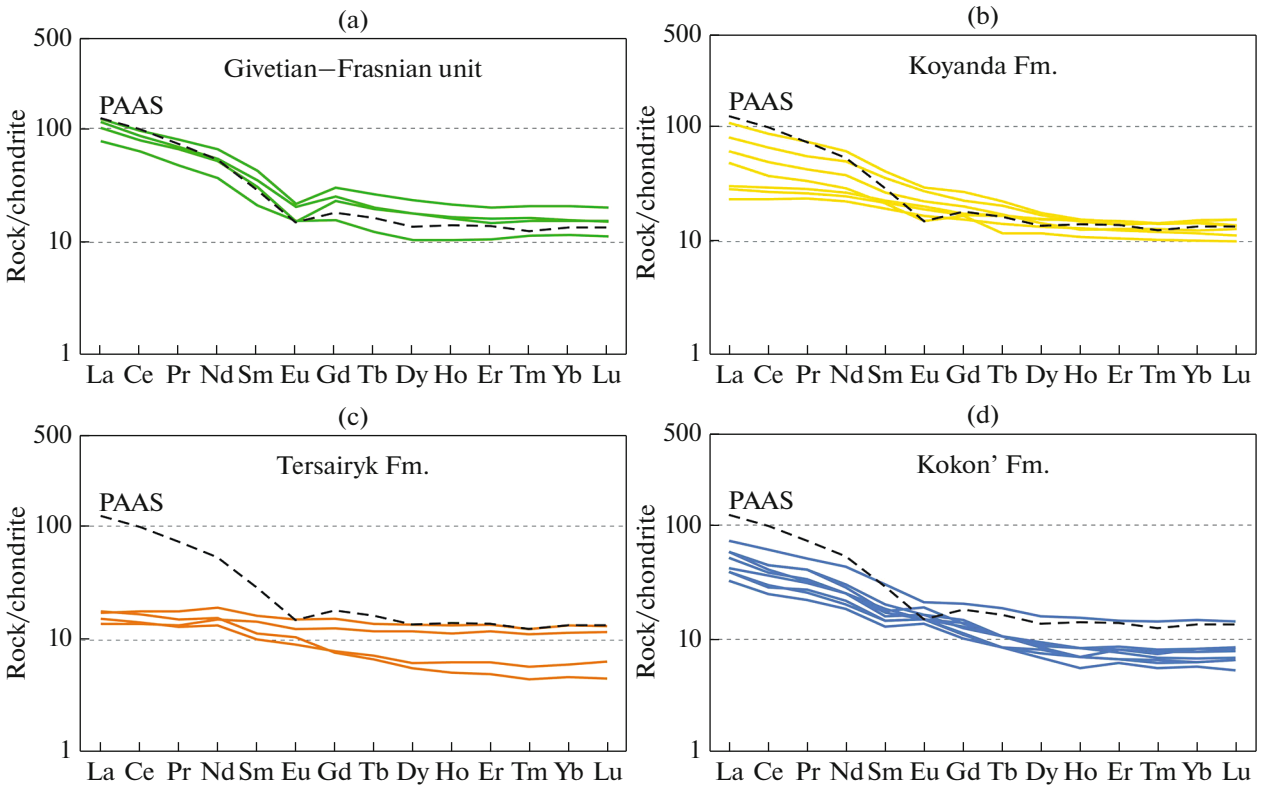

Fig. 10. Chondrite-normalized REE distribution curves: (a)–(d) for rocks of Zharma-Saur island arc zone. Chondrite composition is given after [31]; PAAS, after [61].

mature clayey rocks, composed mainly of clay minerals, have an ICV less than 1.

In the studied sandstones, the ICV values range from 1.15 to 2.51, indicating the supply of immature component into the sedimentation area (see Fig. 9b).

The data suggest erosion of immature material, which corresponds to the composition of eroded rocks, as well as the rapid burial of sediments in close proximity to the province.

The REE distribution pattern in sedimentary and volcanogenic-sedimentary rocks makes it possible to determine the type of source rocks in the provenance area [37, 61]. The REE distribution spectra are differentiated to varying degrees (Fig. 10): from moderate enrichment in LREE relative to HREE for sandstones of the Givetian–Frasnian unit $(La/Yb)_n = 5.95–7.32$, Koyanda Fm. $(La/Yb)_n = 2.01–7.44$ and Kokon' $(La/Yb)_n = 4.76–9.33$ formations, to a flat distribution pattern for tuff sandstones of the Tersairyk Fm. $(La/Yb)_n = 1.20–3.84$.

To compare the REE composition of the sandstones and tuff sandstones under study, we used data on the REE content in the Post-Archean Australian Shale (PAAS), as reported in [61].

The presence of Eu anomaly (Eu/Eu* = 0.57–0.85) and increased content ∑REE = 122–203 ppp is characteristic of sandstones of the Givetian–Frasnian unit and PAAS.

The lower REE contents relative to PAAS and the absence or positive europium anomaly are characteristic of the formations (Fig. 10):

— Koyanda Fm (∑REE = 58–171 ppm, Eu/Eu* = 0.79–1.02);

— Tersairyk Fm (∑REE = 36–54 ppm, Eu/Eu* = 0.92–1.12);

— Kokon Fm (∑REE = 56–131 ppm, Eu/Eu* = 0.86–1.24).

Nd Isotopy

The Nd isotope geochemistry of the sandstones from the Givetian–Frasnian unit and the Kokon' Fm., as well as tuff sandstone from the Koyanda Fm. has been studied (Table 2, Fig. 11).

The $\varepsilon_{Nd}(t)$ value was recalculated using the weighted average age of the youngest detrital zircon population (see Table 1).

Only positive values of $\varepsilon_{Nd}(t)$ were obtained for all studied sandstones and tuff sandstones:

— from +4.48—for sandstone of the Givetian–Frasnian unit;

— from +6.25—for tuff sandstone of the Koyanda Fm., +4.84 for sandstone of the Kokon' Fm. (occupies an intermediate position).

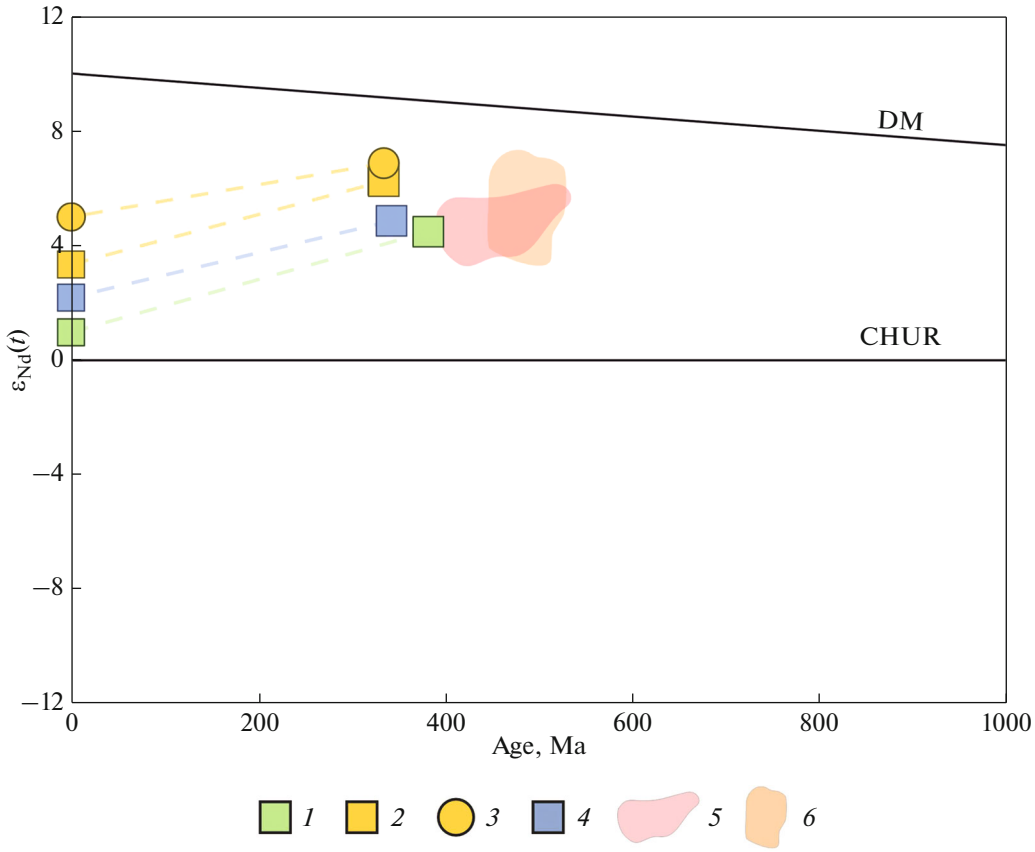

Fig. 11. εNd(*t*)–age diagram plotted for sandstones of Givetian–Frasnian unit, Koyanda and Kokon'formations. (*1*) Sandstone of Givetian–Frasnian unit ($D_2gv–D_3f$); (*2*) tuff sandstone of Koyanda Fm. (C_1kn); (*3*) basalt of Koyanda Fm.; tuff sandstone of Tersairyk Fm. (C_1trs); (*4*) sandstone of Kokon' Fm. (C_1kk); (*5*) Paleozoic granitoids of Chingiz-Tarbagatai zone (after [9]); (*6*) Early Paleozoic volcanic and volcanic-terrigenous deposits of Chingiz-Tarbagatai zone (after [9]).

Sandstones of the Zharma-Saur island arc zone are correlated in terms of the isotopic composition with Paleozoic granitoids, as well as volcanic and volcanogenic-sedimentary rocks of the Chingiz-Tarbagatai zone.

Reconstruction of Paleotectonic Settings

Discriminant diagrams based on petrographic, petrochemical, and geochemical data were used to reconstruct the paleotectonic settings of the formation of the rocks under consideration. Based on the quantitative petrographic analysis of the sandstone samples, a Q–F–R diagram was created to determine the geodynamic conditions of rock formation in the provenance area [39] (Fig. 12a; Supplement 1: Table P2).

The sandstones of the Givetian–Frasnian unit show the relatively highly reworked composition of the province, which falls within the area of the dissected (or deeply eroded) and transitional arc (Fig. 12a).

Tuff sandstones of the Koyanda and Tersairyk formations contain a large volume of weakly erosion-resistant components with a minimum quartz content. Their data points fall into the areas of weakly eroded arc and transition-type arc (Fig. 12a).

The data points of sandstones of the Kokon' Fm. also lie in the transition area and, to a greater extent, in the field of immature arcs (Fig. 12a).

The $15*Al_2O_3–300*TiO_2–Zr$ diagram [45] allows us to trace the reworking process and the degree of

Table 2. Summary table of results of Nd isotope analysis of sandstones and tuff sandstones from Zharma-Sun island arc zone

Sample	Rock	Sm, ppm	Nd, ppm	$^{147}Sm/^{144}Nd$	±2σ	$^{143}Nd/^{144}Nd$	±2σ	$\varepsilon_{Nd}(t)$	t_{Nd} (DM), Ma
Zh19-37	Sandstone	6.27	30.72	0.1234	0.0004	0.512685	0.000005	+4.48	788
Zh19-67	Tuff sandstone	8.71	40.74	0.1292	0.0004	0.512808	0.000015	+6.25	620
Zh19-7	Sandstone	3.35	15.06	0.1346	0.0004	0.512748	0.000009	+4.84	778

$\varepsilon_{Nd}(t)$ values correspond to isotopic composition at a time of 392 Ma (sample Zh19-37), 345 Ma (sample Zh19-67), 352 Ma (sample Zh19-7); composition of homogenous chondrite reservoir (CHUR): $^{147}Sm/^{144}Nd = 0.1967$ and $^{143}Nd/^{144}Nd = 0.512638$ was used to determine $\varepsilon_{Nd}(t)$.

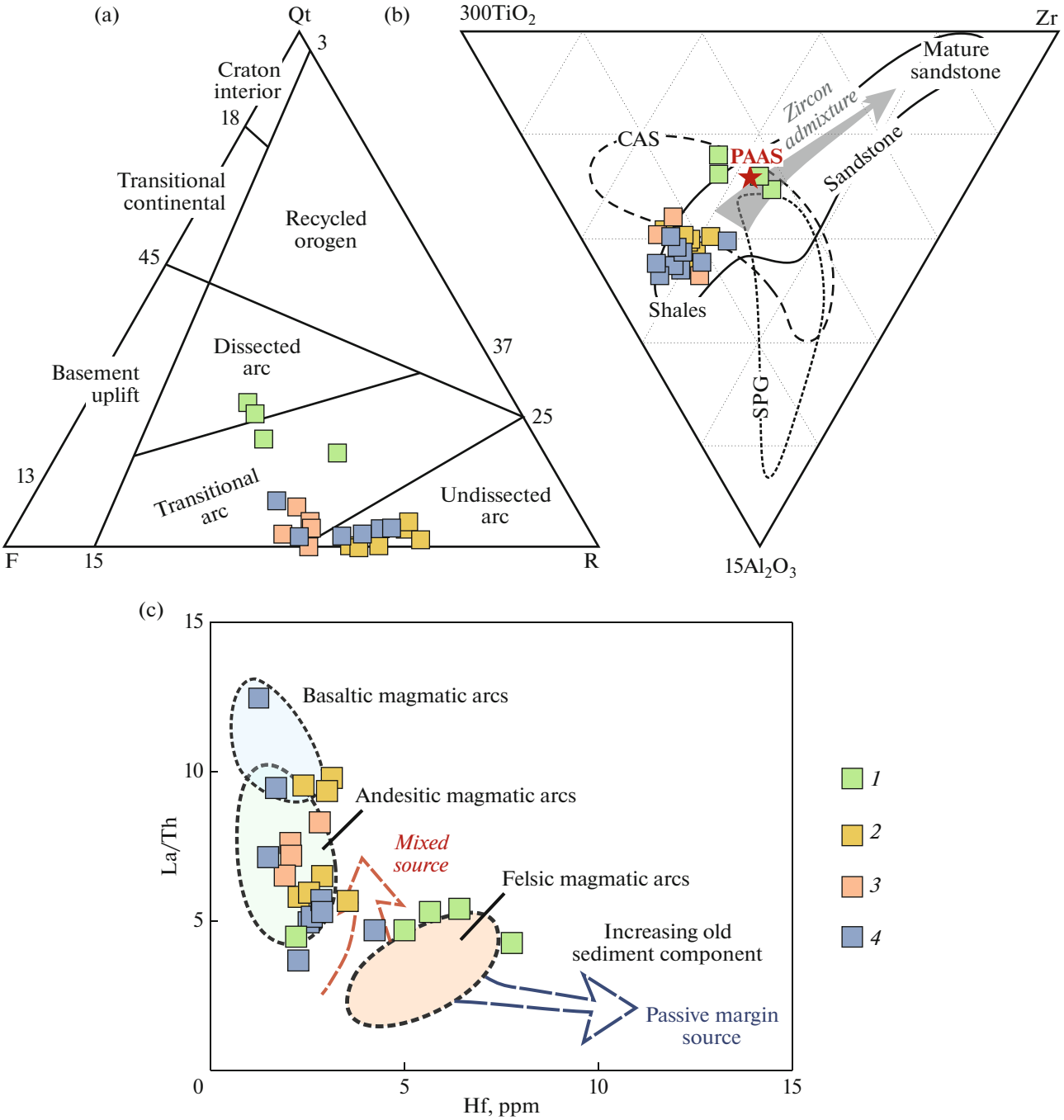

Fig. 12. (a) Qt–F–R diagram for reconstruction of paleotectonic settings (after [39]); (b) $15Al_2O_3$–$300TiO_2$–Zr diagram for determining degree of maturity of clastic material (diagram fields, according to [45]); (c) La/Th–Hf discriminant diagram (after [42]). Notation: CAS, field of calc-alkaline complexes; SPG, stronglyperaluminous granite field; PAAS (after [61]); Qt, total polycrystalline and monocrystalline quartz; F, total feldspars; R, total volcanic and sedimentary rock fragments. (*1*) Sandstones of Givetian–Frasnian unit (D_2gv–D_3f); (*2–3*) tuff sandstones of formations: (*2*) Koyanda (C_1kn), (*3*) Tersairyk (C_1trs); (*4*) sandstones of Kokon' Fm. (C_1kk).

sorting of clastic material, given that the relative proportions of components are transferred from the provenance area with the bulk of sediments (Fig. 12b).

All samples examined show slight variations in the TiO_2/Zr ratio, indicating that there was no long-term rewashing or redeposition of sediments. The sandstones from the Givetian–Frasnian unit differ from other rocks in that they have a higher Zr content. This is likely due to a more acidic magmatic source [49].

In the discriminant diagram (see Fig. 12c), constructed based on the La/Th to Hf ratio [42], data points of the Givetian–Frasnian sandstones are con-

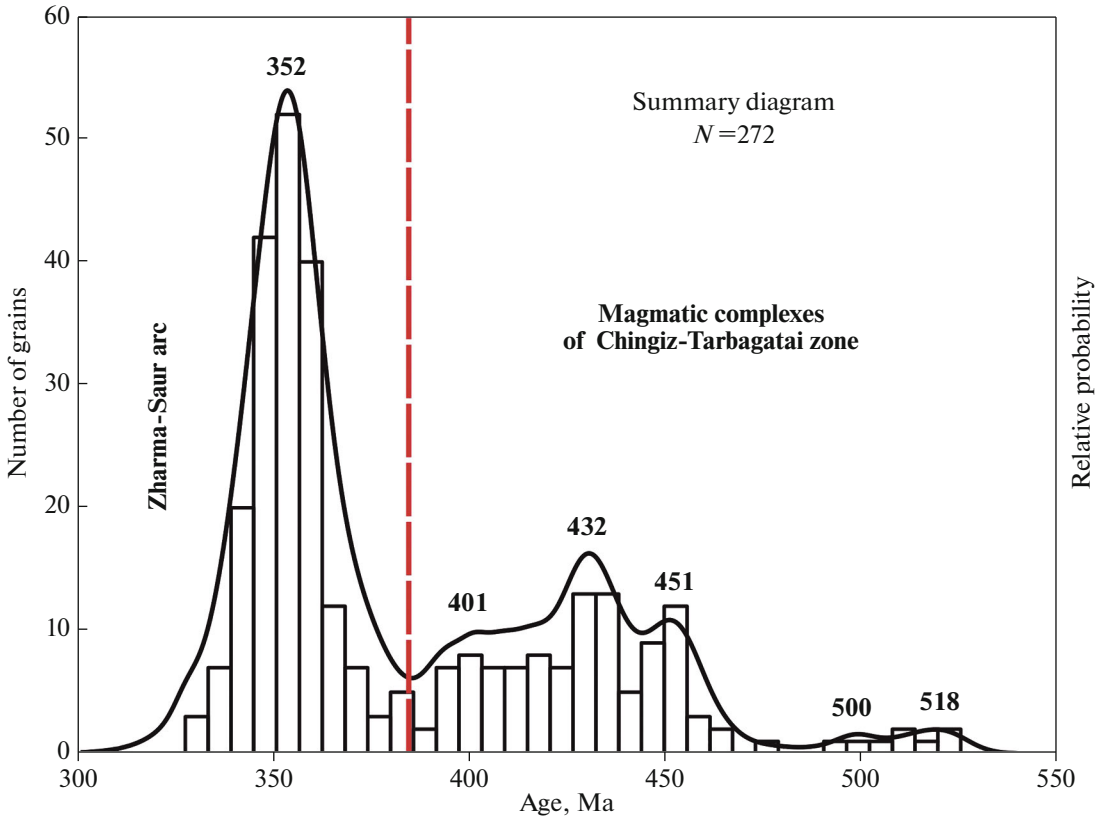

Fig. 13. Summary graph with histogram and relative age probability curve of $^{206}Pb/^{238}U$ ages of detrital zircons from sandstones and tuff sandstones of Zharma-Saur island arc zone. The graph shows the supposed sources of zircons.

fined to the field of rocks formed due to erosion of felsic magmatic rocks, tuff sandstones of the Koyanda and Tersairyk formations are concentrated in the area of data points of andesitic magmatic arcs (Fig. 12c).

The sandstones of the Kokon' Fm. are characterized by a large scatter of data points, from basaltic to andesitic magmatic source. A mixed source is assumed for the silty sandstone sample.

DISCUSSION

Most sandstones are graywackes in their petrochemical composition. This means that they are characterized by the presence of the sodium component (except for the silty sandstone of the Kokon' Fm. with $K_2O > 5$ wt %), as well as a low SiO_2/Al_2O_3 ratio, which determines the degree of rock maturity (see Fig. 8).

The values of petrochemical moduli and their correlation with each other suggest that sandstones and tuff sandstones are similar in chemical composition to the original igneous rocks. This allows us to determine the presence of volcanic material in the provenance area (see Fig. 9a).

The ICV calculation results suggest the presence of rocks that have not undergone intense weathering during transportation to the sedimentary area (Fig. 9b). Sandstones from the Givetian–Frasnian sequence are characterized by a higher CIA compared to other sandstones, indicating more altered rocks of the feeding province.

The REE composition of the rocks of the Givetian-Frasnian sequence is similar to that of the PAAS, indicating the relative maturity of the rocks of this sequence (see Fig. 10).

The sandstones of the Koyanda, Tersairyk, and Kokon' formations are located below the PAAS level and differ in their spectral distribution patterns, which may indicate a less intense reworking of clastic materials and a closer chemical composition to igneous rocks from the province.

The study of the Nd isotopy has shown that the rocks have a primitive composition with positive $\varepsilon_{Nd}(t)$ values ranging from +4.48 to +6.25. This suggests the presence of juvenile igneous rocks in the province, without any ancient crustal material (Fig. 11). These isotopic characteristics are similar to those of the Paleozoic granitoids, as well as volcanic and volcanosedimentary rocks in the Chingiz-Tarbagatai region.

The accumulation of the Givetian_Frasnian sandstones occurred due to the erosion of a relatively acidic and reworked source, as indicated by the higher quartz content in the clasts, the SiO_2 and Zr contents, as well as the distribution of rock data points on the discriminant diagrams of paleotectonic environments (Fig. 12;

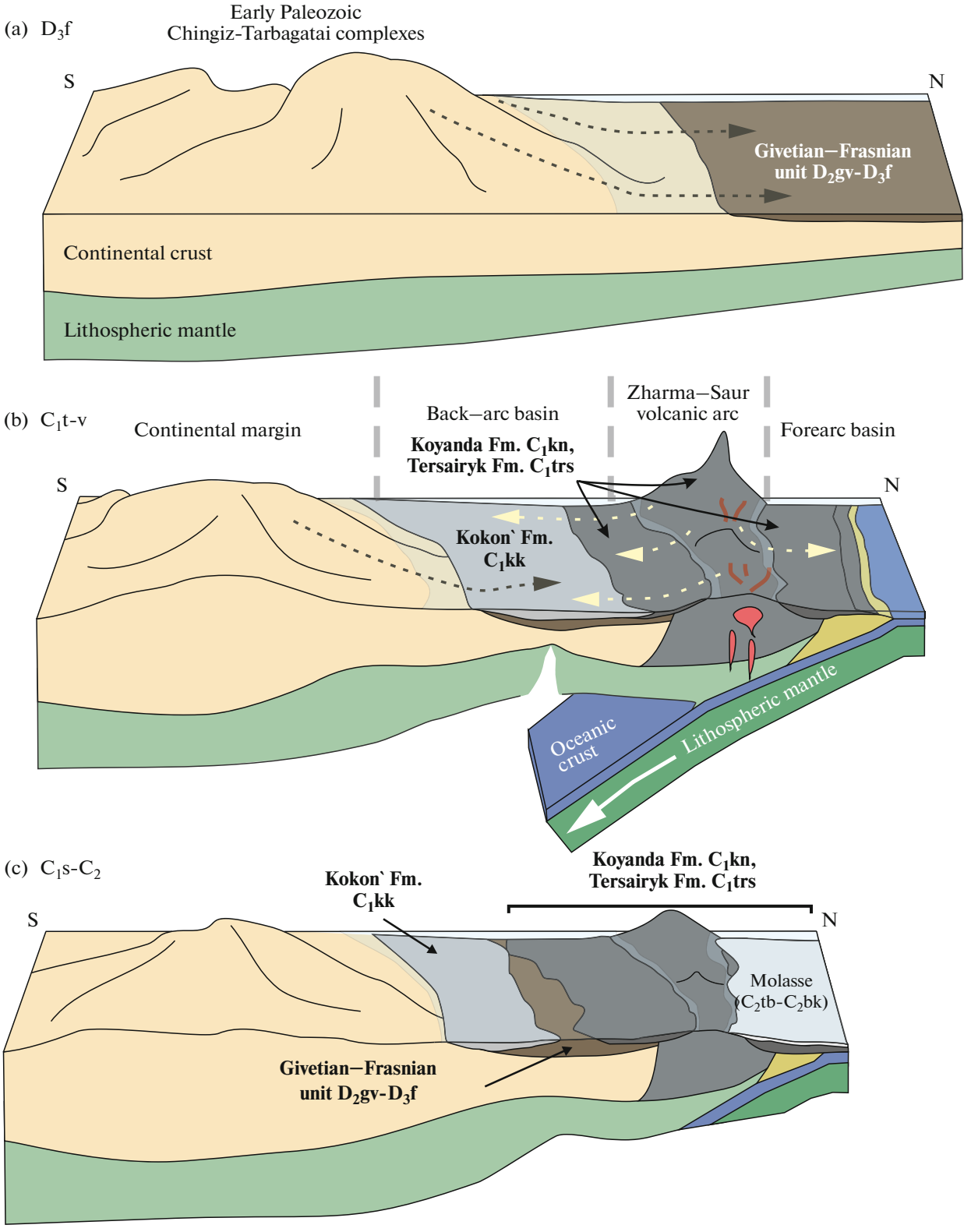

Fig. 14. Schematic geodynamic profiles for Late Devonian–Carboniferous stage of evolution of Chingiz-Tarbagatai zone (in modern coordinates). (a) Frasnian Age of Late Devonian; (b) Tournaisian-Visean of Early Carboniferous); (c) Serpukhovian Age of Early Carboniferous–Middle Carboniferous. The Middle Carboniferous molasse is composed of the Tauba (C_2tb) and Bukon' (C_2bk) formations [14, 17]. Inferred direction of sediment drift is shown by dotted arrows.

Supplement 1: Table P2, Table P3). The results of the U–Pb dating of detrital zircons suggest that the Cambrian, Ordovician-Silurian, and Early Devonian magmatic complexes, which are common within the conjugate Chingiz-Tarbagatai zone, were the sources of clastic material for the formation of these sandstones (Figs. 5a, 13, 14a).

The tuff sandstones of the Koyanda and Tersairyk formations are characterized by lower CIA values and lower quartz content in the clasts, as well as higher $\varepsilon_{Nd}(t)$ values (Table 2; Figs. 9b, 11).

The U–Pb dating of the tuff sandstones of the Koyanda and Tersairyk formations has allowed us to confirm their Early Carboniferous age, which was previously considered conditional or insufficiently supported. At the same time, the unimodal distribution of dates in the interval from the Famennian to the Tournaisian indicates that the rocks formed as a result of the destruction of a predominantly Late Paleozoic provenance area: the Zharma-Saur island arc (Figs. 13, 14b). Such isotope-geochemical evidence suggests a change in the provenance of the rocks in the Famennian time. In the paleotectonic reconstruction diagrams, the sandstones of the Kokon' Fm. are located between sandstones of the Givetian–Frasnian unit and tuff sandstones of the Koyanda and Tersairyk formations (Figs. 12a, 12b). The Kokon' Fm. was accumulated as a result of simultaneous destruction of the rock complexes of Early Paleozoic complexes of the Chingiz-Tarbagatai zone and the Early Carboniferous Zharma-Saur arc. This is confirmed by both U–Pb dates and Nd-isotope data (Figs. 5d, 11, 13, 14b). The formation of the trough that was filled with deposits from the Kokon' Fm. occurred simultaneously with volcanic activity within the Zharma-Saur volcanic arc region. This trough was located in the back part of the island-arc system and was most likely formed due to back-arc extension as the oceanic lithosphere subsided beneath the Zharma-Saur volcanic arc towards the Kazakhstan Paleocontinent.

According to the results of U–Pb dating of detrital zircons, the formation of the Middle–Late Devonian sandstones (Givetian–Frasnian) of the Zharma-Saur island arc zone occurred due to the destruction of Early Paleozoic provenance areas. The age peaks coincide with the stages of volcanic activity and granite formation within the Chingiz-Tarbagatai zone [9] (Fig. 13). This suggests that the emplacement of the Zharma-Saur island arc zone occurred in close proximity to the Chingiz-Tarbagatai zone (Fig. 14a). However, this raises doubts about the existence of a significant ocean basin that separated the Zharma-Saur island arc from the Early Paleozoic island-arc complexes in the Chingiz-Tarbagatai region until the Early Carboniferous period [34, 35, 56, 60, 65]. Also, the summary graph of detrital zircon ages records the beginning of magmatism of the Zharma-Saur volcanic arc from the Famennian time (see Fig. 13).

Consequently, we suggest that the foundation of the Zharma-Saur volcanic arc occurred in the Famennian age within the northeastern margin of the Kazakhstan Paleocontinent, which is recorded by the change in the source of clastic material for sedimentary and volcanogenic-sedimentary rocks.

CONCLUSIONS

The petrographic study and petro-geochemical analysis of sandstones and tuff sandstones have allowed us to determine the composition and type of the provenance areas. U–Pb isotope dating has enabled us to pinpoint the interval of island-arc volcanism, the age of rocks in the provinces, and establish the maximum depositional age.

(1) The formation of the Givetian–Frasnian unit in the Zharma-Saur volcanic arc zone occurred as a result of erosion of Early Paleozoic rocks of the Chingiz-Tarbagatai zone.

(2) Magmatism within the Zharma-Saur volcanic arc zone began during the Famennian–Visean and became more intensive in the Tournaisian.

(3) The studied rocks of the Koyanda and Tersairyk formations were formed as a result of the erosion of rocks from the Zharma-Saur island arc region. The provinces for the sedimentary rocks of the Kokon' Fm. could be simultaneously the both the Early Paleozoic formations of the Chingiz-Tarbagatai area and the Early Carboniferous igneous complexes of the Zharma-Saur volcanic arc area.

(4) The formation of the Zharma–Saur volcanic arc zone occurred at the northeastern margin of the Kazakhstan Paleocontinent during the Late Devonian–Early Carboniferous.

SUPPLEMENTARY INFORMATION

The online version contains supplementary material available at https://doi.org/10.1134/S0016852124700274.

ACKNOWLEDGMENTS

The authors thank Academician K.E. Degtyarev for his invaluable assistance in preparing this article, D.V. Alexeiev for their useful comments, and the editor of *Geotectonics* M.N. Shoupletsova for thorough editing.

FUNDING

U–Pb geochronological study and determination of the contents of major and trace elements and Nd isotope composition were supported by the Russian Science Foundation (project no. 22-77-00061). Petrographic study of volcanic and volcanic-terrigenous rocks was performed within the state assignment of IGM SB RAS (no. 122041400044-2).

CONFLICT OF INTEREST

The authors of this work declare that they have no conflicts of interest.

REFERENCES

1. N. A. Berzin, R. G. Coleman, N. L. Dobretsov, L. P. Zonenshain, S. Syuchan', and E. Z. Chang, "Geodynamic map of the western part of the paleo-Asian ocean," Russ. Geol. Geophys. **35** (7–8), 8–28 (1994).
2. S. M. Beskin, V. M. Larin, and Yu. B. Marin, *Rare-metal Granitoid Formations* (Nauka, Leningrad, 1979).
3. N. I. Volkova, E. N. Tarasova, N. V. Polyanskii, A. G. Vladimirov, and V. D. Khomyakov, "High-pressure rocks in the serpentinite melange of the Chara zone, Eastern Kazakhstan: Geochemistry, petrology, and age," Geochem. Int. **46**, 386–401 (2008).
4. *The 1 : 500 000 Geological Map of the Kazakh SSR. Eastern Kazakhstan Ser. Explanatory Note* (Mingeo SSSR, Alma-Ata, 1979).
5. The 1 : 200000 Geological Map of Eastern Kazakhstan. Zaisan Ser. Sheet M-44-XXXIV. Explanatory Note (TOO GRK "Topaz," Ust'-Kamenogorsk 2014).
6. K. E. Degtyarev, *Tectonic Evolution of the Early Paleozoic Active Margin in Kazakhstan*, Ed. by Yu. G. Leonov, A. G. Akhmetiev, Yu. O. Gavrilov, Yu. V. Karyakin, S. A. Kurenkov, and M. A. Semikhatov (Nauka, Moscow, 1999) [in Russian].
7. K. E. Degtyarev, *Tectonic Evolution of the Early Paleozoic Island Arc Systems and the formation of Continental Crust of Caledonides of Kazakhstan*, Ed. by M. A. Fedonkin, M. A. Akhmetiev, Yu. O. Gavrilov, Yu. V. Karyakin, Yu. G. Leonov, M. A. Semikhatov, S. D. Sokolov, and M. D. Khutorskii (GEOS, Moscow, 2012) [in Russian].
8. K. E. Degtyarev and A. V. Ryazantsev, Cambrian arc-continent collision in the Paleozoides of Kazakhstan," Geotectonics **41**, 63–86 (2007).
9. K. E. Degtyarev, K. N. Shatagin, V. P. Kovach, and A. A. Tret'yakov, "The formation processes and isotopic structure of continental crust of the Chingiz Range Caledonides (Eastern Kazakhstan)," Geotectonics **49**, 485–514 (2015).
10. A. N. Didenko, A. A. Mossakovskii, D. M. Pecherskii, C. B. Ruzhentsov, and T. N. Kheraskov, Geodynamics of Paleozoic oceans in Central Asia," Geol. Geofiz. **35** (7–8), 59–75 (1994).
11. A. N. Didenko and O. L. Morozov, "Geology and paleomagnetism of Middle–Upper Paleozoic rocks of the Saur Ridge," Geotectonika **4**, 64–80 (1999).
12. N. L. Dobretsov and M. M. Buslov, "Late Cambrian–Ordovician tectonics and geodynamics of Central Asia," Russ. Geol. Geophys. **48** (1), 71–82 (2007).
13. P. V. Ermolov, E. P. Izokh, A. P. Ponomareva, and V. D. Tyan, *Gabbro-Granite Series in the Western Part of the Zaisan Fold System*, Ed. by N. L. Dobretsov and E. P. Izokh (Nauka, Novosibirsk, 1977) [in Russian].
14. G. Zh. Zholtayev, O. I. Nikitina, V. Ya. Zhaimina, E. Yu. Seitmuratova, T. E. Pirogova, N. I. Ivanova, E. M. Fazylov, E. S. Musina, S. A. Nigmatova, and B. U. Baishashov, "Stratigraphic charts of the Phanerozoic of Kazakhstan. Explanatory note)," in *Decisions of the Meeting on the Unification of Stratigraphic Charts of the Phanerozoic of Kazakhstan, Almaty, November 25–29, 2021. Part 1: Paleozoic* (TOO "378", Almaty, 2021).
15. N. G. Karmanova and N. S. Karmanov, "Universal X-ray fluorescence technique for silicate analysis of rocks using ARL-9900XP spectrometer," in *Proceedings of VII All-Russia X-ray Spectral Analysis Conference. Novosibirsk, September 19–23, 2011* (Nauka, Novosibirsk, 2011).
16. A. A. Mossakovskii, S. V. Puzhentsev, S. G. Samygin, and T. N. Kheraskova, "The Central Asian Orogenic Belt: Geodynamic evolution and history of formation," Geotektonika, No. 6, 3–33 (1993).
17. *Decisions of the III Kazakhstan Stratigraphic Conference on the Precambrian and Phanerozoic, Alma-Ata, 1986 with Regional Stratigraphic Schemes. Part I. Precambrian and Paleozoic,* Ed. by A. A. Abdulin, I. F. Nikitin, and I. I. Nikitchenko (St. Petersburg, 1991).
18. A. V. Ryazantsev, "Structures of the Middle Paleozoic active margin in Kazakhstan: lateral series, migration," Dokl. Earth Sci. **369** (5), 659–663 (1999).
19. S. G. Samygin and T. N. Kheraskova, "Geological structure and stages of tectonic evolution of the Paleozoides of Kazakstan," Litosfera **19** (3), 347–371 (2019).
20. N. A. Sevryugin, "Geological structure of the Semipalatinsk area," Sov. Geol. No. 7, 5–20 (1959).
21. L. V. Sergeeva, "Devonian deposits in the northern Chingiz Region," Litosfera, No. 2, 81–93 (2004).
22. V. E. Khain, Tectonics of Continents and Oceans, Ed. by V. E. Khain (Nauchn. Mir, Moscow, 2001) [in Russian].
23. S. V. Khromykh, P. D. Kotler, and D. V. Semenova, "Geochemistry, age and geodynamic setting of formation of the Saur abbro-granitoid intrusive series (Vostochnyi Kazakhstan)," Geosfernye Issled., No. 2, 6–26 (2019).
24. S. V. Khromykh, "Basic and associated granitoid magmatism and geodynamic evolution of the Altai accretion–collision system (Eastern Kazakhstan)," Russ. Geol. Geophys. **63** (3), 279–299 (2022).
25. V. D. Shutov, "Classification of sandstones," Litol. Polezn. Iskop., No. 5, 86-103 (1967).
26. G. N. Shcherba, B. A. D'yachkov, N. I. Stuchevskii, G. P. Nakhtigal', A. N. Antonenko, and V. N. Lyubetskii, The Greater Altai (Geology and Metallogeny) (Gylym, Almaty 1998).
27. Ya. E. Yudovich and M. P. Ketris, Foundations of Lithochemistry, Ed. by V. N. Shvanov, V. T. Frolov, and Yu. A. Tkachev (Nauka, St. Petersburg, 2000) [in Russian].
28. A. Abrajevich, R. Van der Voo, N. M. Levashova, and M. L. Bazhenov, "Palaeomagnetism of the mid-Devonian Kurgasholak Formation, Southern Kazakhstan: Constraint on the Devonian paleogeography and oroclinal bending of the Kazakhstan volcanic arc," Tectonophysics **441**, 67–84 (2007).
29. D. V. Alexeiev, A. V. Ryazantsev, A. Kröner, A. A. Tretyakov, X. Xia, and D. Y. Liu, "Geochemical data and zircon ages for rocks in a high-pressure belt of Chu-Yili Mountains, southern Kazakhstan: Implications for the

earliest stages of accretion in Kazakhstan and the Tianshan," J. Asian Earth Sci. **42**, 805–820 (2011).

30. N. A. Berzin and N. L. Dobretsov, "Geodynamic evolution of Southern Siberia in Late Precambrian-Early Paleozoic time," in *Reconstruction of the PaleoAsian Ocean*, Ed. by R. G. Coleman (VSP Int. Sci. Publ., Utrecht, The Netherlands, 1994), pp. 53–70.
31. W. V. Boynton, "Cosmochemistry of the rare earth elements: Meteorite studies," in *Rare Earth Element Geochemistry*, Ed. by P. Henderson (Elsevier, Amsterdam, 1984), pp. 63–114.
32. M. M. Buslov, T. Watanabe, Y. Fujiwara, K. Iwata, L. V. Smirnova, I. Y. Safonova, N. N. Semakov, and A. P. Kiryanova, "Late Paleozoic faults of the Altai region, Central Asia: Tectonic pattern and model of formation," J. Asian Earth Sci. **23** (5), 655–671 (2004).
33. M. M. Buslov, I. Yu. Safonova, T. Watanabe, O. Obut, Y. Fujiwara, K. Iwata, N. N. Semakov, Y. Sugai, L. V. Smirnova, and A. Yu. Kazansky, "Evolution of the Paleo-Asian Ocean (Altai–Sayan region, Central Asia) and collision of possible Gondwana-derived terranes with the southern marginal part of the Siberian continent," Geosci. J. **5**, 203–224 (2001).
34. Y. Chen, W. Xiao, B. F. Windley, J. E. Zhang, K. Zhou, and M. Sang, "Structures and detrital zircon ages of the Devonian–Permian Tarbagatay accretionary complex in west Junggar, China: Imbricated ocean plate stratigraphy and implications for amalgamation of the CAOB," Int. Geol. Rev. **59** (9), 1097–1115 (2016).
35. Y. Chen, W. Xiao, B. F. Windley, J. E. Zhang, M. Sang, R. Li, S. Song, and K. Zhou, "Late Devonian-early Permian subduction-accretion of the Zharma-Saur oceanic arc, West Junggar (NW China): Insights from field geology, geochemistry and geochronology," J. Asian Earth Sci. **145**, 424–445 (2017).
36. R. Cox and D. R. Lowe, "A conceptual review of regional-scale controls on the composition of clastic sediment and the coevolution of continental blocks and their sedimentary cover," J. Sediment. Res., No. 1, 1–12 (1995).
37. R. L. Cullers, "The controls on the major and trace element variation of shales, siltstones, and sandstones of Pennsylvanian–Permian age from uplifted continental blocks in Colorado to platform sediment in Kansas, USA," Geochim. Cosmochim. Acta **58**, 4955–4972 (1994).
38. W. R. Dickinson, L. S. Beard, G. R. Brakenridge, J. L. Erjavec, R. C. Ferguson, K. F. Inman, R. A. Knepp, F. A. Lindberg, and P. T. Ryberg, "Provenance of North American Phanerozoic sandstones in relation to tectonic setting," GSA Bull. **94**, 222–235 (1983).
39. W. R. Dickinson and G. E. Gehrels, "Use of U–Pb ages of detrital zircons to infer maximum depositional ages of strata: A test against a Colorado Plateau Mesozoic database," Earth Planet. Sci. Lett. **288**, 115–125 (2009).
40. N. L. Dobretsov, N. A. Berzin, and M. M. Buslov, "Opening and tectonic evolution of the Paleo-Asian Ocean," Int. Geol. Rev. **37**, 335–360 (1995).
41. I. B. Filippova, V. A. Bush, and A. N. Didenko, "Middle Paleozoic subduction belts: the leading factor in the formation of the Central Asian fold-and-thrust belt," Rus. J. Earth Sci. **3**, 405–426 (2001).
42. P. A. Floyd and B. E. Leveridge, "Tectonic environment of the Devonian Gramscatho basin, south Cornwall: framework mode and geochemical evidence from turbiditic sandstones," J. Geol. Soc. **144**, 531–542 (1987).
43. R. L. Folk, P. B. Andrews, and D. W. Lewis, "Detrital sedimentary rock classification and nomenclature for use in New Zealand," N. Z. J. Geol. Geophys. **13**, 937–968 (1970).
44. R. L. Folk, *Petrology of Sedimentary Rocks* (Hemphill Publ. Comp., Austin, USA, 1980).
45. D. Garcia, M. Fonteilles, and J. Moutte, "Sedimentary fractionations between Al, Ti, and Zr and the genesis of strongly peraluminous granites," J. Geol. **102**, 411–422 (1994).
46. L. M. Heaman, R. Bowins, and J. Crocket, "The chemical composition of igneous zircon suites: Implications for geochemical tracer studies," Geochem. Cosmochem. Acta **54**, 1597–1607 (1990).
47. G. A. Jenner, H. P. Longerich, S. E. Jackson, and B. J. Fryer, "ICP-MS – a powerful tool for high precision trace element analysis in earth sciences: evidence from analysis of selected U.S.G.S. reference samples," Chem. Geol. **83**, 133–148 (1990).
48. P. D. Kotler, S. V. Khromykh, A. V. Zakharova, D. V. Semenova, A. V. Kulikova, A. G. Badretdinov, E. I. Mikheev, and A. S. Volosov, "Model of the formation of monzogabbrodiorite–syenite–granitoid intrusions by the example of the Akzhailau Massif (Eastern Kazakhstan)," Petrology **32** (2), 179–200 (2024).
49. A. Kröner, V. Kovach, E. Belousova, E. Hegner, R. Armstrong, A. Dolgopolova, R. Seltmann, D. V. Alexeiev, J. E. Hofmann, J. Wong, M. Sun, K. Cai, T. Wang, Y. Tong, S. A. Wilde, K. E. Degtyarev, and E. Rytsk, "Reassessment of continental growth during the accretionary history of the Central Asian Orogenic Belt," Gondwana Res. **25**, 103–125 (2014).
50. K. R. Ludwig, *User's Manual for Isoplot 3.00: A Geochronological Toolkit for Microsoft Excel, 2003, No. 4.* https://homepages.see.leeds.ac.uk/~ear6clif/Manual2.3.pdf.
51. M. Montenari, *Stratigraphy and Timescales* (Keele Univ., Newcastle, UK, 2016, Vol. 1).
52. H. W. Nesbitt and G. M. Young, "Early Proterozoic climates and plate motions inferred from major element chemistry of lutites," Nature **299**, 715–717 (1982).
53. Y. Orihashi and T. Hirata, "Rapid quantitative analysis of Y and REE abundances in XRF glass bead for selected GSJ reference rock standards using Nd-YAG 266 nm UV laser ablation ICP-MS," Geochem. J. **37**, 401–412 (2003).
54. C. Paton, J. D. Woodhead, J. C. Hellstrom, J. M. Hergt, A. Greig, and R. Maas, "Improved laser ablation U–Pb zircon geochronology through robust downhole fractionation correction," Geochem. Geophys. Geosyst., No. 11, Q0AA06 (2010). https://doi.org/10.1029/2009GC002618
55. F. J. Pettijohn, *Sedimentary Rocks* (Harper & Row, NY, CD, USA, 1972).

56. I. Safonova, A. Perfilova, O. Obut, P. Kotler, S. Aoki, T. Komiya, B. Wang, and M. Sun, "Traces of intra-oceanic arcs recorded in sandstones of eastern Kazakhstan: implications from U–Pb detrital zircon ages, geochemistry, and Nd–Hf isotopes," Int. J. Earth Sci. **111** (8), 2449–2468 (2021).

57. I. Safonova and A. Perfilova, "Survived and disappeared intra-oceanic arcs of the Paleo-Asian Ocean: evidence from Kazakhstan," Nat. Sci. Rev. **10** (2) (2023). https://doi.org/10.1093/nsr/nwac215

58. P. Shen, Y. Shen, X. H. Li, H. Pan, H. Zhu, L. Meng, and H. Dai, "Northwestern Junggar basin, Xiemisitai mountains, China: a geochemical and geochronological approach," Lithos **140**, 103–118 (2012).

59. J. Sláma, J. Košler, D. J. Condon, J. L. Crowley, A. Gerdes, J. M. Hanchar, M. S. A. Horstwood, G. A. Morris, L. Nasdala, N. Norberg, U. Schaltegger, N. Schoene, M. N. Tubrett, and M. J. Whitehouse, "Plešovice zircon – a new natural reference material for U–Pb and Hf isotopic microanalysis," Chem. Geol. **249** (1–2), 1–35 (2008).

60. S. Song, W. Xiao, B. F. Windley, A. S. Collins, Y. Chen, J. Zhang, K. Schulmann, C. Han, B. Wan, S. Ao, Z. Zhang, D. Song, and R. Li, "Late Paleozoic Chingiz and Saur arc amalgamation in West Junggar (NW China): Implications for accretionary tectonics in the Southern Altaids," Tectonics **39**, 1–24 (2020).

61. S. T. Taylor and S. M. McLennan, *The Continental Crust: Composition and Evolution* (Blackwell, Oxford, UK, 1985).

62. M. Wiedenbeck, P. Alle, F. Corfu, W. L. Griffin, M. Meier, F. Oberli, A. V on Quadt, J. C. Roddick, and W. Spiegel, "Three natural zircon standards for U–Th–Pb, Lu–Hf, trace element and REE analyses," Geostand. Newsl., No. 19, 1–23 (1995).

63. B. F. Windley, D. V. Alexeiev, W. Xiao, A. Kröner, and G. Badarch, "Tectonic Models for Accretion of the Central Asian Orogenic Belt," J. Geol. Soc. London **164** (1), 31–47 (2007).

64. Y. Xu, B. F. Han, W. Liao, and A. Li, "The Serpukhovian–Bashkirian amalgamation of Laurussia and the Siberian continent and implications for assembly of Pangea," Tectonics **41**, e2022TC007218 (2022). https://doi.org/10.1029/2022TC007218

65. Y. F. Zhu and X. Xu, "The discovery of Early Ordovician ophiolite mélange in Taerbahatai Mts., Xinjiang, NW China," Acta Petrol. Sin. **22** (12), 2833–2842 (2006).

Translated by D. Voroshchuk